



Influences of Shot Peening Parameters on Mechanical Properties and Fatigue Behavior of 316 L Steel: Experimental, Taguchi Method and Response Surface Methodology

Erfan Maleki¹ · Okan Unal² · Kazem Reza Kashyzadeh³

Received: 3 December 2020 / Accepted: 11 March 2021 / Published online: 30 August 2021
© The Author(s) 2021

Abstract

Severe plastic deformation methods like shot peening (SP) are known as efficient surface treatments and grain refining processes which afford more effective properties in metallic materials. In the current research, a comprehensive study was carried out on SP of AISI 316 L steel. It included 42 different SP treatments with a wide range of Almen intensities of 12–27 A and various coverage degrees (100%–1500%). Several experimental tests were conducted in order to explore the microstructure, grain size, surface topography, hardness, wettability, and residual stresses of the specimens. Next, two different approaches including Taguchi method (TM), and response surface methodology (RSM) were deployed for modeling, analysis, and optimization. RSM and TM were used to examine the influence of the effective parameters. Based on the optimized results, the fatigue behavior of the selected treatments was investigated experimentally in both smooth and notched specimens.

Keywords AISI 316L stainless steel · Shot peening · Simulation · Optimization

Abbreviations

| | |
|------|------------------------------------|
| CRS | Compressive residual stress |
| NS | Nanostructured |
| UFG | Ultrafine-grained |
| SPD | Severe plastic deformation |
| SSPD | Surface severe plastic deformation |
| SP | Shot peening |
| CSP | Conventional shot peening |
| SSP | Severe shot peening |
| ABSP | Air blast shot peening |
| RSM | Response surface methodology |
| TM | Taguchi method |
| WCA | Water contact angle |
| DOE | Design of experiment |
| RDI | Regulated deficit irrigation |

| | |
|-------|---|
| OM | Optical microscopy |
| FESEM | Field emission scanning electron microscopy |
| BSE | Back scatter electron |
| EDX | Energy-dispersive X-ray spectroscopy |
| EBSD | Electron backscatter diffraction |
| XRD | X-ray diffraction |
| RMSE | Root mean square of error |

1 Introduction

Metallic biomaterials are extensively used in bio-applications such as pharmaceutical and textile industries and surgical implants. AISI 316L stainless steel is widely employed in aerospace, food, and chemical, as well as biomaterial industries, due to its strong corrosion resistance in aggressive environments and its exceptional biocompatibility [1–3]. Compared to other metals and alloys, the biomaterial of 316L austenitic stainless steel is one of the most commonly used materials for fracture fixation devices due to its distinctive mechanical properties and its low cost [4, 5]. The biomaterial of stainless steel 316L is self-protected by the spontaneous formation of a thin oxide film. It has been used in wire form for neurosurgical clips, artificial hip, surgical sutures, and microvascular clips (to cure aneurysms) [6, 7]. Besides, this grade of austenitic stainless steel is applicable in producing vascular stents and

✉ Erfan Maleki
erfan.maleki@polimi.it

¹ Department of Mechanical Engineering, Politecnico di Milano, 20156 Milan, Italy

² Mechanical Engineering Department, Karabuk University, 78050 Karabuk, Turkey

³ Department of Transport, Academy of Engineering, Peoples' Friendship University of Russia (RUDN), 117198 Moscow, Russia

electrodes and conducting lead wires. Pulse generator housing of cardiac pacing systems is another area where stainless steel 316L is commonly used [8, 9].

316L stainless steel does not harden in reaction to heat treatments [10–13]. However, it can be hardened by cold working, post-processing, and grain refinement treatments which are aimed at obtaining desirable mechanical properties [14–17].

Generally, grain refinement brings about a reduction in the size of the grain (coarse grains of the material) so that it reaches a submicron (< 1000 nm) scale. Grains with a size of 1–100 nm and 100–500 nm are called nanostructured (NS) and ultrafine-grained (UFG), respectively [18]. In their microstructure, NS and UFG materials are featured by a very high density of grain boundaries, which can play a significant role in the development and exhibition of superior properties. Compared with UFG metals or alloys, the most considerable properties of NS grains are their high yield and fracture strength as well as their superplastic behavior at relatively low temperatures and high strain rates. Furthermore, NS metals depict a high strain rate sensitivity, compared to UFG materials [19, 20].

Shot peening (SP) is one of the popular approaches in grain refinement. Specially, it is considered one of the surface severe plastic deformation (SSPD) methods. SP is a cold working process whereby small shots are thrust at the surface of a material at a certain velocity. A single shot mechanically deforms the material by creating a dimple when it strikes the surface [21, 22].

There exist two main parameters in the SP process, including Almen intensity and surface coverage. Based on the values of Almen intensity and coverage and the overall severity of peening, one could have either a conventional shot peening (CSP) or a severe shot peening (SSP). There is an extensive body of research concerning the effects of CSP on the improvement of different materials [23–27]. In the SSP process, unconventionally high Almen intensities and coverages are employed to introduce more compressive residual stresses and to refine the grains of surface layer of the treated material [28, 29]. SSP is generally used for nanocrystallization of the surface [30–33]. Moreover, other types of shot peening treatments, using ultrasonic waves to create vibrational excitation of the shots, have been used for this purpose [34, 35]. However, to carry out SSP, three approaches have so far been proposed: increasing Almen intensity at a very high range [36, 37], increasing coverage beyond 100% (or 200%) [38, 39], and heightening both Almen intensity and coverage simultaneously [40–42].

Recently, Bagherifard et al. [43] and Al-Janabi et al. [44] have proved that the performance of the treated materials of

magnesium alloy AZ31 and AISI 304 in the bio environment such as biocompatibility and wettability increases significantly as a result of applying SSP. Moreover, regarding the application of SSP to steel AISI 316 L, Bagherifard et al. [45, 46] in their other research revealed that the mechanical properties and the application of this material are finely enhanced in severely treated specimens, in comparison with specimens which had been treated conventionally. In both studies, they applied two different SP treatments (Almen intensity of 15A and coverage of 100% for CSP and Almen intensity of 7C and coverage of 1500% for SSP). They also studied mechanical properties including roughness, hardness, residual stress, wettability, as well as some cell-based and bacterial assays. Moreover, Li et al. have studied the effect of Rotational Accelerated Shot Peening (RASP) as an innovative surface nanocrystallization technique on the microstructure of 316 L stainless steel [47].

Considering the above discussion, since the beneficial effects of SP on steel AISI 316 L have been established [45–47] and because of its diverse applications, the authors of the current study have attempted to conduct a comprehensive study on steel AISI 316 L biomaterial in order to shed more light on this process and the way it should be analyzed under different circumstances. The aim is to scrutinize the effects of 42 different SP treatments with varying Almen intensities of 12–27 A and distinct coverages of 100%–1500%—conventional to severe—on surface morphology, surface hardness, residual stress, surface roughness, and surface wettability of 316L biomaterial. As for the main novelty of this work, besides the tests, experimental results were analyzed and optimized with two different approaches, namely response surface methodology (RSM), and Taguchi method (TM) as follow for parametric analysis and optimization.

2 Experimental Procedure

2.1 Material and Specimens

Commercial AISI 316L stainless steel was chosen as specimen material and its chemical composition is shown in Table 1. The supplied sheets of the material were mechanically ground and polished to achieve mirror finishing. Then, ASTM E8M [48] and ASTM E466 [49] standards were applied to fabricating tensile and fatigue test specimens, respectively, with a thickness of 6 mm. Figure 1 presents the shape and size of the related specimens.

Tensile tests were performed at room temperature as well as the strain rate of 0.06 mm/mm/min by utilizing a clip gauge extensometer with a parallel length of 25 mm. The

Table 1 Chemical composition of AISI 316 L stainless steel (weight %)

| C | Mn | Si | Cr | Cu | Mo | Ni | S | Co | P | S | Fe |
|-------|------|------|-------|------|------|-------|-------|------|-------|-------|-----|
| 0.022 | 1.34 | 0.47 | 17.11 | 0.41 | 2.03 | 10.15 | 0.005 | 0.26 | 0.034 | 0.001 | Bal |

stress–strain diagrams are illustrated for three specimens in Fig. 2. Also, the key parameters of these diagrams are reported in Table 2. The yield stress was calculated based on the strain offset of 0.2%. The average value of elastic modulus was estimated around 212 GPa. Figure 3 represents the typical microstructure of the employed material. The solute banding lines can be observed clearly using Nomarski contrast. The average grain size was 130 μm (without twins) or 110 μm (including twins) as determined by stereological methods.

2.2 Shot Peening Treatments

An air blast shot peening (ABSP) device was used to execute 42 distinct SP treatments on the specimens. All treatments were performed by using standard steel shots with an average hardness of 48–50 HRC, impingement angle of 90° , nozzle diameter of 6.35 mm (1/4 in), and a nozzle-sample distance equal to 10 cm. The high Almen intensities ranged from 12, 15, 18, 21, 24, to 27A (0.01 mm). The corresponding high range of coverage for these intensities was 100, 250, 500, 750, 1000, 1250, and 1500%. Almen intensity was calculated through the SAE J443 standard [50].

Fig. 1 Shape and size of the specimens for different tests including **a** tensile specimen, **b** smooth fatigue specimen, and **c** notched fatigue specimen

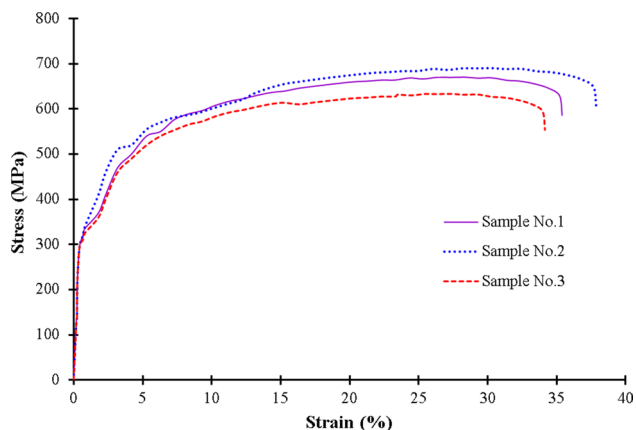
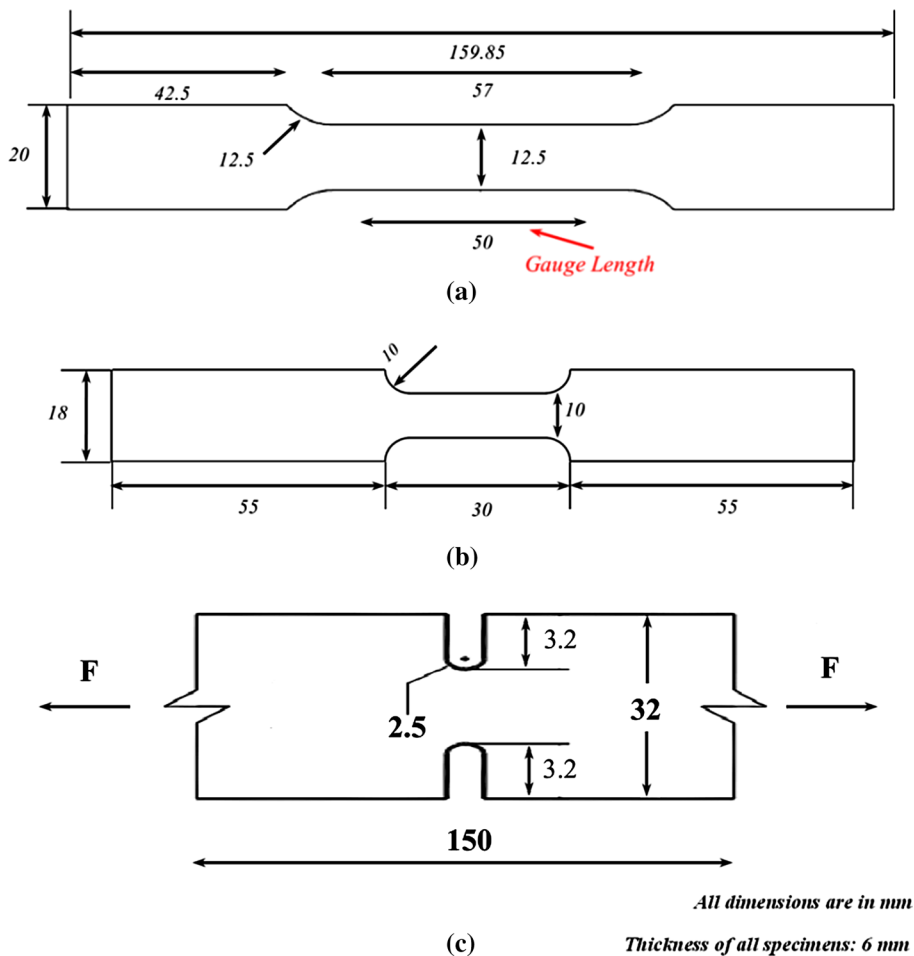


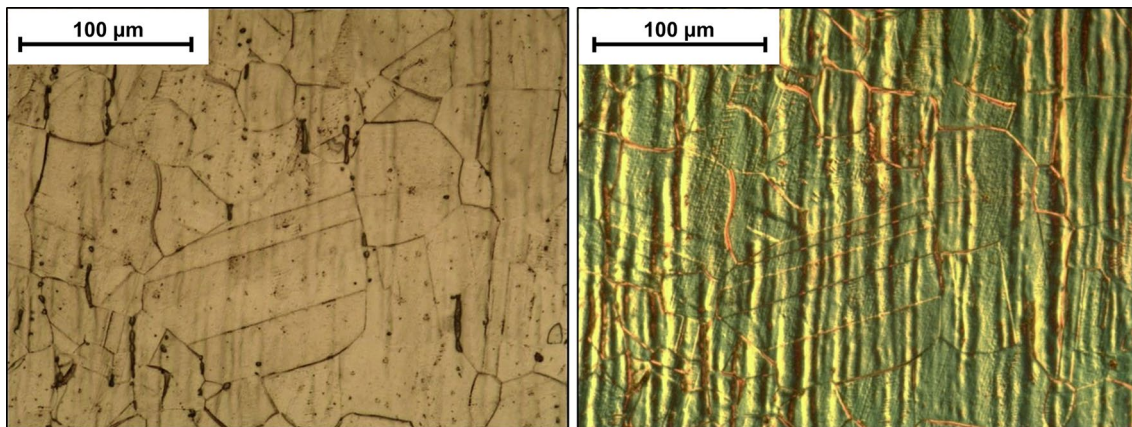
Fig. 2 Stress–strain diagram of three specimens for 316L stainless steel

2.3 Microscopic Observations

For microstructural evolution, the samples of each series were cross-sectioned, impregnated in a Phenolic hot mounting resin, and ground with a series of SiC papers up to P4000 (average scratch size of 5 μm). Afterward, the cross-sections

Table 2 Key parameters of stress–strain diagrams

| Item | Ultimate stress point | | Break stress point | | |
|--------------|-----------------------|-------------|--------------------|-------------|-------------|
| | Stress (MPa) | Strain (%) | Stress (MPa) | Strain (%) | |
| Specimen no. | 1 | 670.2878989 | 28.3284298 | 585.9773234 | 35.38602905 |
| | 2 | 690.3965359 | 30.31142 | 601.5566431 | 37.863052 |
| | 3 | 633.4220945 | 27.33693 | 557.7485706 | 34.1475218 |
| Delta | | 56.9744414 | 2.97449 | 43.8080725 | 3.7155302 |
| Deviation | | 28.89501626 | 1.514535834 | 22.20632381 | 1.891855684 |
| Mean | | 664.7021764 | 28.6589266 | 581.7608457 | 35.79886762 |

**Fig. 3** Typical microstructure of the employed steel 316L, (left) conventional optical microscopy and (right) optical microscopy with Nomarski contrast

were polished individually through polycrystalline diamond water-based suspensions which had an average scratch size equal to 1 mm and 0.25 mm. Microstructure examinations were performed using OM and FESEM. Furthermore, Olympus and Mira 3-XMU software were used for OM and FESEM observations, respectively. It is possible to reach high resolution up to 1.0 nm at 30 keV by Mira 3-XMU. Besides, 200 V to 30 kV accelerating voltage exists with a BSE detector, as well as EDX and EBSD facilities. The samples were etched using Marble's reagent (compositions: CuSO_4 , Hydrochloric Acid and Water) for 5 s.

2.4 XRD Grain Size Measurements

XRD measurements were performed to determine the grain size after applying SP treatments at a higher severity. To do the XRD analysis, the authors used the X'Pert PRO MPD (PANalytical) X-ray diffractometer system in conjunction with the X'Pert High Score Plus (V. 3) analyzer with $\text{Cu K}\alpha$ radiation. This was operated at 40 kV and 40 mA, scanning angle of 30° – 150° , and irradiated area of 10 mm. The full width at half maximum (FWHM) of the diffraction θ peaks were obtained, and crystallite sizes were calculated using Scherer's equation [51]:

$$d_{XRD} = K\lambda/\beta\cos\theta \quad (1)$$

where d is the apparent size of crystal, λ stands for the wavelength of x-radiation (i.e. $\lambda_{\text{Cu-K}\alpha}$ 1.54 Å), B signifies the corrected FWHM (i.e. region below the curve which is divided by the maximum radian height), θ represents the diffraction angle, and K denotes a constant close to unity (i.e. 0.94). β can be obtained from the observed FWHM by convoluting the Gaussian profile modeling specimen broadening β_r :

$$\beta_r^2 = \beta_0^2 - \beta_i^2 \quad (2)$$

where β_0 is the observed broadening, and β_i is the instrumental broadening.

2.5 Microhardness Measurements

Microhardness experiments were carried out (up to 800 μm on the cross-sectional surface within 20 μm intervals) to explore the impact of the applied SP treatments on hardness. Qness GmbH Q30 A microhardness tester at a load of 10 gf with a duration of 7 s using Vickers indenter.

2.6 Surface Roughness Measurements

A common side effect of SP process influencing fatigue behavior, surface roughness of specimens is calculated through SURFCORDER SE500. The definition of ISO 4287 was employed to analyze roughness parameters [52].

2.7 Residual Stress Measurements

Multiple XRD analyses were conducted using Xstress 3000 G2/G2R X-ray Stress Analyzer (radiation Cr K α , an irradiated area of 4 mm diameter, $\sin^2\psi$ method, and diffraction angle of $(2\theta) \sim 156$ scanned between 45 and -45) in order to investigate the impact of residual stresses on the specimens. The observations were performed in depth step by stepwise via taking away a thin layer of material ($\sim 40 \mu\text{m}$). This removal was accomplished by electro-polishing with an acetic acid (94%) and perchloric acid (6%) solution.

2.8 Wettability Measurements

The water contact angle was studied to explore surface wettability via Krüss DSA 100 by sessile drop technique, and image analysis (OCA-20, Dataphysics Instruments). A pipette was used to pour approximately 2 μL of ultrapure distilled water into the samples. The data were recorded by taking 10 different measurements from the surfaces. Additionally, the average value of the static contact angle was calculated.

(Specimen preparation for microstructural evolution and other experiments is schematically illustrated in Appendix 1.)

2.9 Fatigue Test

The SANTAM SAF-250 universal test machine was used to carry out fatigue test under tension-tension loading conditions. The mean stress was considered a positive value, and the stress ratio of $R = 0.1$. The loading frequency of 20 Hz was applied to all fatigue tests. In the present study, 20 fatigue test samples were employed to develop the S–N diagram for each treatment and SP conditions. The fatigue test was performed at 10 different stress levels. Hence, the mean fatigue life of the two specimens was considered as the fatigue life at the corresponding cyclic load level [53]. The number of cycles to failure increases by decreasing stress amplitude until the S–N curve turns into a horizontal line at a particular limiting stress. This value is the fatigue limit endurance upto which the material can bear an infinite number of cycles without failure [54, 55]. The fatigue limit endurance may be measured through the JSME S 002 standard [56] and using the staircase method.

3 Response Surface Methodology

Response surface methodology (RSM) is both a statistical and mathematical approach for modeling, analysis, and optimization of real engineering problems. Here, optimization is performed by making a detailed analysis of the responses in terms of several input variables. RSM has been particularly useful in manufacturing and materials sciences for several decades. Metal cutting processes take advantage of RSM optimization [57, 58]. In addition, RSM has entered materials sciences [59]. With regard to SP, prevention of Almen strip wastes and time during the detection of pre-shot peening conditions make the usability of statistical methods meaningful. Therefore, RSM is applied to optimize Almen intensity in terms of surface roughness, surface residual stress, surface nanocrystallization, and surface mechanical properties [60, 61]. In this study, the influence of Almen intensity (A) and surface coverage (B) was determined on the deformed layer thickness, surface microhardness, surface roughness, surface residual stress, maximum compressive residual stress, and water contact angle (WCA).

$$\text{Depth of deformed layer: } f(A, B) \quad (3)$$

$$\text{Surface microhardness: } f(A, B) \quad (4)$$

$$\text{Surface roughness: } f(A, B) \quad (5)$$

$$\text{Surface residual stress: } f(A, B) \quad (6)$$

$$\text{Maximum compressive residual stress: } f(A, B) \quad (7)$$

$$\text{Water contact angle: } f(A, B) \quad (8)$$

RSM is depicted by response surface “Y” as a second order polynomial regression equation.

$$Y = b_0 + \sum b_i x_i + \sum b_{ii} x_i^2 + \sum b_{ij} x_i x_j + e_r \quad (9)$$

4 Taguchi Method

Different Design of Experiments (DOE) methods have been proposed to reduce the number of tests and laboratory costs associated with classifying effective parameters in each process. The results of this analysis can be used to determine the most important effective parameter as well as ineffective parameters on the response. In the last decade, many studies have been done to optimize SP parameters such as shot size, speed, pressure, and nozzle distance by using the Taguchi method. In this research, tensile strength, surface roughness,

and surface residual stress were considered as an optimization target function.

Sun et al. [62] have optimized laser peening parameters by using FEM and Taguchi approach. Three different parameters including laser power, pulse width, and laser spot diameter have been used as the inputs, and surface residual stress has been considered an output. Pathak and Munjadas [63] have optimized parameters of SP process on the Al 2024 alloy specimens. They reported the effects of shot size, shot velocity, impact angle, and shot distance on surface residual stress and surface roughness. Besides, the effects of shot peening parameters (shot diameter, speed, and duration of treatment as time) have been investigated on the surface roughness and tensile strength of AA 6061 [64]. Jamaluddin et al. [65] have improved the quality of shot blasting process by applying Taguchi approach and performing various tests. Empirical studies have been done on the SP parameters for welded austenitic stainless steel in association with surface hardness and static strength [66]. In addition to the above parameters, flow rate is also considered an important and effective parameter of SP process [67]. The effects of SP parameters on the ultimate strength of low carbon steel have been explored by carrying out tensile tests on v-notched specimens (angle and depth of notch are 45 degree and 2 mm, respectively) [68].

As a novelty of the present research, TM, one of the most common DOE techniques, has been used to perform a comprehensive study into the impact of shot peening parameters on metallurgical and mechanical properties

of 316L stainless steel biomaterial. To this end, a large number of experiments were carried out. Two effective variables of SP treatment including Almen intensity and surface coverage were used at the five different levels to create Taguchi algorithm as shown in Fig. 4.

Table 3 shows the symbols used for the variables as the control factors and their level of test. In the present analysis, an L25 orthogonal array was used to run the experiment as indicated in Table 4.

Moreover, various outputs were investigated and it was revealed that increasing the value of some outputs (type I) and reducing the value of some others (type II) produce beneficial effects.

Type I outputs include depth of deformed layer, surface microhardness, surface residual stress, and maximum residual stress.

Type II outputs include surface roughness and surface wettability.

Here, in order to maximize outputs type I, the larger-the-better type is employed to calculate S/N ratios using Eq. (10) [69–71]:

$$(S/N)_{max} = -10\text{Log} \left[\frac{1}{n} \sum_{i=1}^{i=n} 1/y_i^2 \right] \tag{10}$$

where y_1, y_2, \dots, y_n stands for the bent angles calculated in the bending process, and every bending condition is repeated n times. Also, in order to minimize outputs type II, the smaller-the-better type is employed to calculate S/N ratios using Eq. (11):

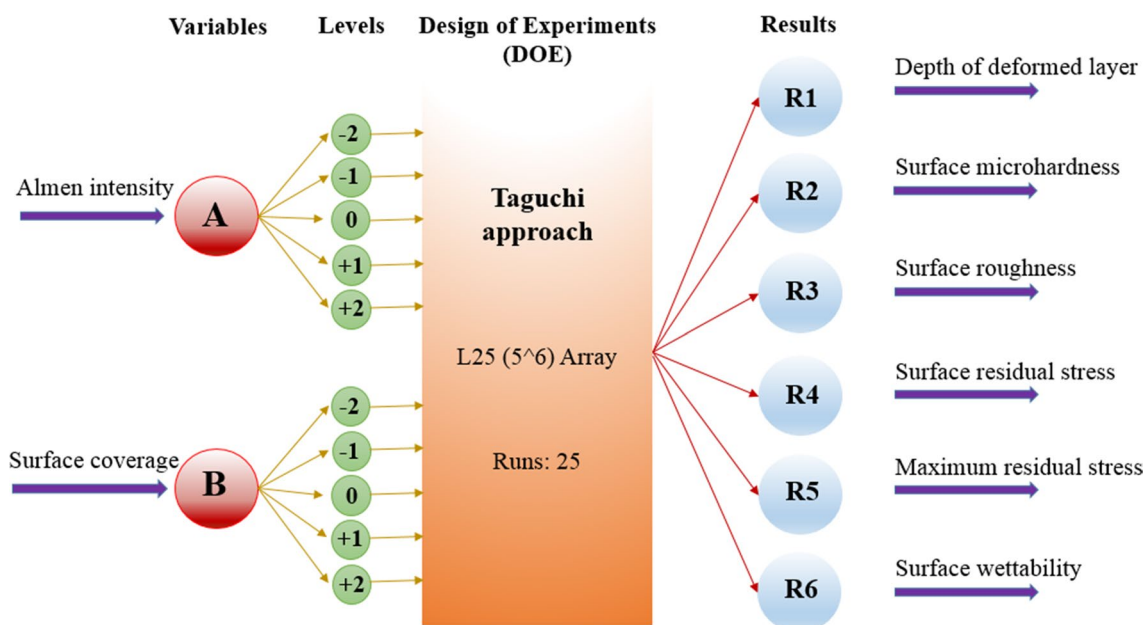


Fig. 4 Conceptual structural of TM according to the considered input and output parameters

Table 3 Variables and levels set for TM at the shot peening process

| Symbols | Controlled factor | Levels | | | | |
|---------|-------------------|--------|------|-----|------|------|
| | | (−2) | (−1) | (0) | (+1) | (+2) |
| A | Almen intensity | 12 | 18 | 21 | 24 | 27 |
| B | Surface coverage | 100 | 250 | 500 | 1000 | 1500 |

Table 4 The L25 orthogonal array and its combination setting for different factors and experimental results

| Run no. | Controlled factor | | | | Experimental results | | | |
|---------|-------------------|----|-----|-----|----------------------|------|------|------|
| | A | B | R1 | R2 | R3 | R4 | R5 | R6 |
| 1 | −2 | −2 | 35 | 326 | 2.93 | −264 | −348 | 70.0 |
| 2 | −2 | −1 | 47 | 341 | 2.97 | −270 | −366 | 69.5 |
| 3 | −2 | 0 | 61 | 368 | 2.89 | −278 | −392 | 69.0 |
| 4 | −2 | +1 | 91 | 388 | 2.82 | −281 | −411 | 68.0 |
| 5 | −2 | +2 | 107 | 400 | 2.79 | −297 | −416 | 66.0 |
| 6 | −1 | −2 | 51 | 362 | 3.26 | −294 | −467 | 69.5 |
| 7 | −1 | −1 | 62 | 378 | 3.33 | −311 | −483 | 68.0 |
| 8 | −1 | 0 | 73 | 399 | 3.37 | −315 | −489 | 67.0 |
| 9 | −1 | +1 | 112 | 421 | 3.30 | −326 | −497 | 65.0 |
| 10 | −1 | +2 | 137 | 433 | 3.26 | −323 | −511 | 61.0 |
| 11 | 0 | −2 | 54 | 371 | 3.43 | −316 | −498 | 68.0 |
| 12 | 0 | −1 | 70 | 394 | 3.47 | −317 | −511 | 66.0 |
| 13 | 0 | 0 | 80 | 416 | 3.55 | −319 | −523 | 65.0 |
| 14 | 0 | +1 | 127 | 447 | 3.50 | −339 | −544 | 63.0 |
| 15 | 0 | +2 | 151 | 454 | 3.42 | −353 | −569 | 59.0 |
| 16 | +1 | −2 | 60 | 381 | 3.63 | −328 | −533 | 66.5 |
| 17 | +1 | −1 | 72 | 407 | 3.66 | −341 | −557 | 64.0 |
| 18 | +1 | 0 | 86 | 438 | 3.74 | −354 | −577 | 63.0 |
| 19 | +1 | +1 | 140 | 464 | 3.71 | −373 | −598 | 61.0 |
| 20 | +1 | +2 | 166 | 474 | 3.61 | −368 | −606 | 57.0 |
| 21 | +2 | −2 | 64 | 391 | 3.73 | −347 | −570 | 65.0 |
| 22 | +2 | −1 | 78 | 421 | 3.79 | −355 | −585 | 62.5 |
| 23 | +2 | 0 | 96 | 448 | 3.84 | −368 | −589 | 61.0 |
| 24 | +2 | +1 | 146 | 477 | 3.81 | −383 | −628 | 59.0 |
| 25 | +2 | +2 | 177 | 489 | 3.68 | −391 | −652 | 56.0 |

$$(S/N)_{min} = -10 \log \left[\frac{1}{n} (y_1^2 + y_2^2 + \dots + y_n^2) \right] \quad (11)$$

In order to compare the results of various output parameters with different dimensions, Regulated Deficit Irrigation (RDI) is used as a dimensionless method that is based on maximum and minimum values of the solution as follows Eq. (12) [72]:

$$RDI = \frac{|Methodsol - Bestsol| \times 100}{|Maxsol - Minsol|} \quad (12)$$

5 Results and Discussion

5.1 Experimental Results

5.1.1 Microstructural Characterization

Cross-sectional OM images of plastically deformed specimen's surfaces after applying SP treatments are shown in Fig. 5. The figure depicts OM observations for all of the considered intensities and four coverages of 100, 500, 1000, and 1500% for each respective Almen intensities. It can be seen that by increasing the severity of the SP process through raising the values of Almen intensity and coverage, the depth of the plastic deformation in the surface layer improves as well. Figure 6 exhibits

the FESEM images of shot peened specimens. In Fig. 6a, c, the change in the effect of surface coverage could be identified at the constant Almen intensities of 12A and 27A, respectively. The lowest and highest conditions of Almen intensity indicate the capability of surface coverage within the context of layer depth and nanocrystallization. Figure 6c shows effective nanocrystallization on behalf of the highest Almen intensity and coverage. Since at the

same magnification, the structurally evolved layer covers the surface on solely. In Fig. 6b, different Almen intensities of 15, 18, 21, and 24A have been compared at the same value of coverage (75%). It can be observed that by increasing intensity and coverage simultaneously, grain refinement in the surface layer improves, and by increasing intensity, surface roughness rises.

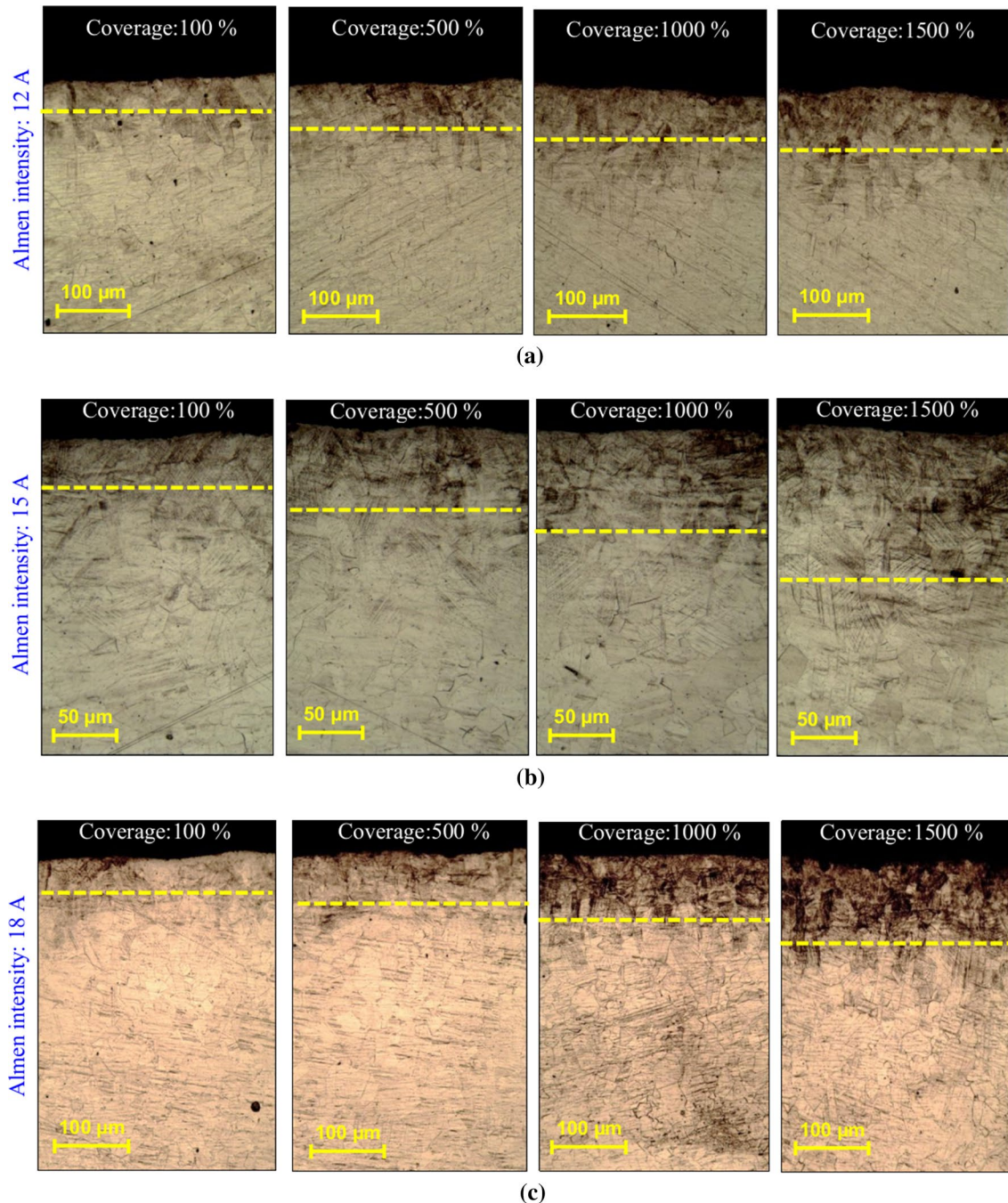


Fig. 5 Cross-sectional OM images of the treated specimens with different Almen intensities of **a** 12A, **b** 15A and **c** 18A with different coverages of 100, 500, 1000, and 1500%

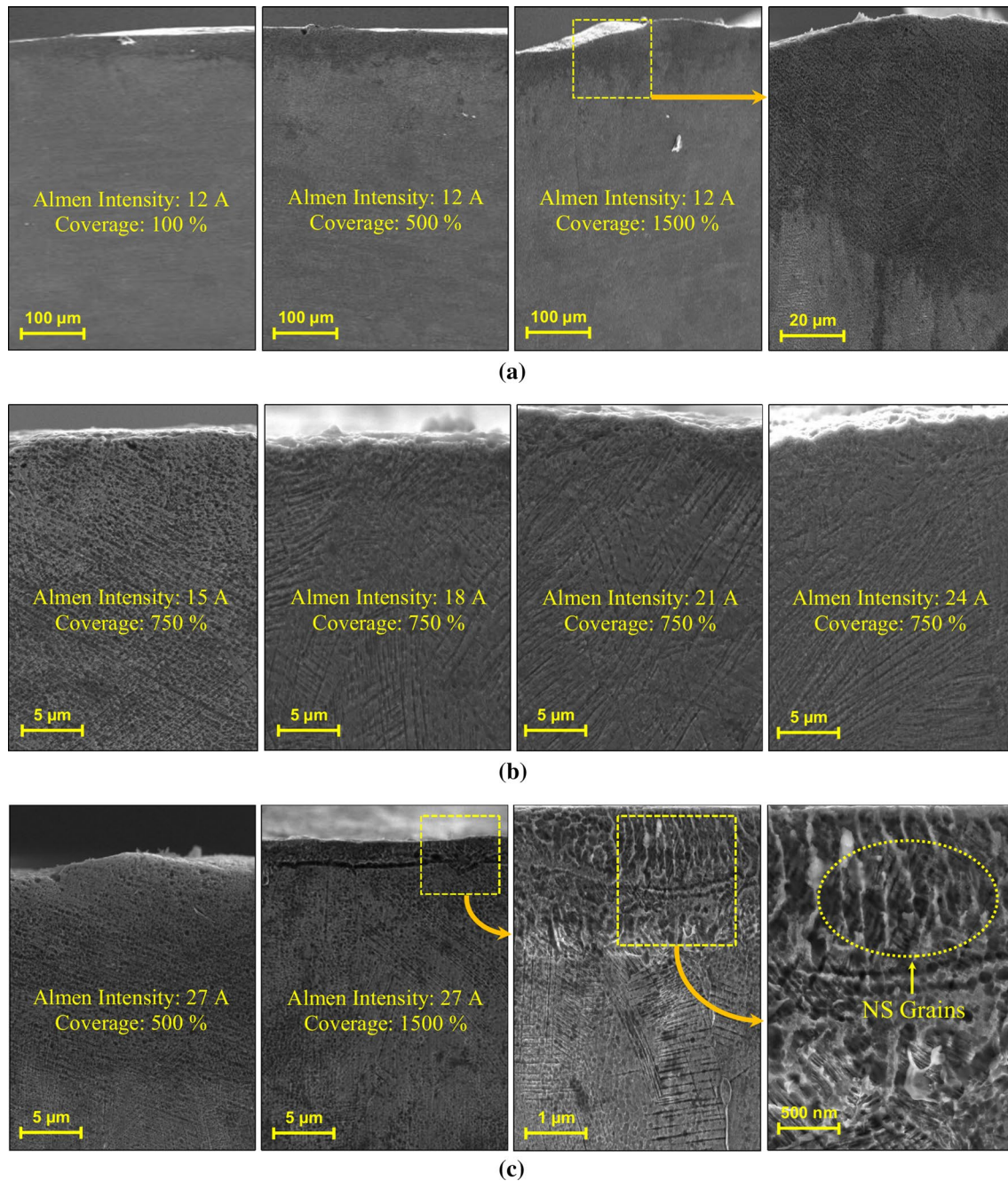


Fig. 6 FESEM observations of the shot peened specimens: **a** treated specimens with same intensity of 12 A with different coverages, **b** treated specimens with different intensities of 15, 18, 21, and 24 A

with same coverage of 750%, and **c** treated specimens with same intensity of 27 A with different coverages of 500 and 1500% with respect to creation of the NS grains in the surface layer

In order to have a better understanding about the condition of grain refinement by the SP process at a high severity, highly magnified FESEM images of some of the considered samples with Almen intensities of 15, 18, 21, and 24 A and the highest coverage of 1500% have been presented in Fig. 7. The created UFG and NS grains and layers, that reducing grain sizes to the refined grains scale, clearly realized near the top surface layer. As reported by Chamanfar

et al. [73], and Bagherifard et al. [45], this layer, representing a brittle white layer near the surface, is considered to be the fine-grained layer. Notwithstanding the existence of a fine-grained layer, it is possible to trigger cracks to nucleate and initiate on this layer. The presence of the unetchable properties complicates determining the structure of compounds or phases on this layer, although it is fairly hard and thermally stable [74]. Also, Saitoh et al. have demonstrated

that the sharp boundaries between NS and UFG layers can be observed [75]. Although surface nanocrystallization by the SSP process was revealed through FESEM observations, XRD measurements were performed to achieve a greater certainty in this regard and to determine the size of the surface grains. Treated specimens with the highest coverage (1500%) were chosen for each considered intensity. The XRD patterns of treated specimens are displayed in Fig. 8. As mentioned, the crystallite sizes of specimens in the surface layer were determined by Scherer's equation based on the value of FWHM of a diffraction peak (Table 5).

5.1.2 Measurements in Plastically Deformed Layer

Different experimental measurements of hardness, roughness, residual stress, and wettability were carried out in the plastically deformed surface layer. Moreover, the results of microstructural characterization were used to calculate the depth of the deformed layer. The depth of this layer of coarse grains (similar to the grains of the not shot peened material) can be considered as the depth of the deformed layer [76, 77]. In this study, an average of seven times measurements

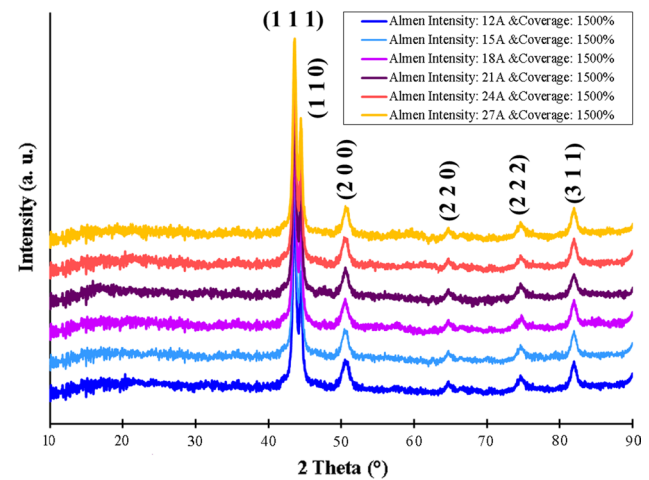


Fig. 8 Intensity distribution of all severely treated specimens with coverage of 1500%

of depth in different areas was regarded as the depth of the deformed layer. As an example, determination of the depth of deformed layer for the shot peened specimen having an

Fig. 7 FESEM observations with higher magnifications with respect to creation of the UFG and NS grains and layers, sharp boundaries and refined and coarse grains for the treated specimens with **a** Almen intensity of 15A and coverage of 1500%, **b** Almen intensity of 18A and coverage of 1500%, **c** Almen intensity of 21A and coverage of 1500%, and **d** Almen intensity of 24A and coverage of 1500%

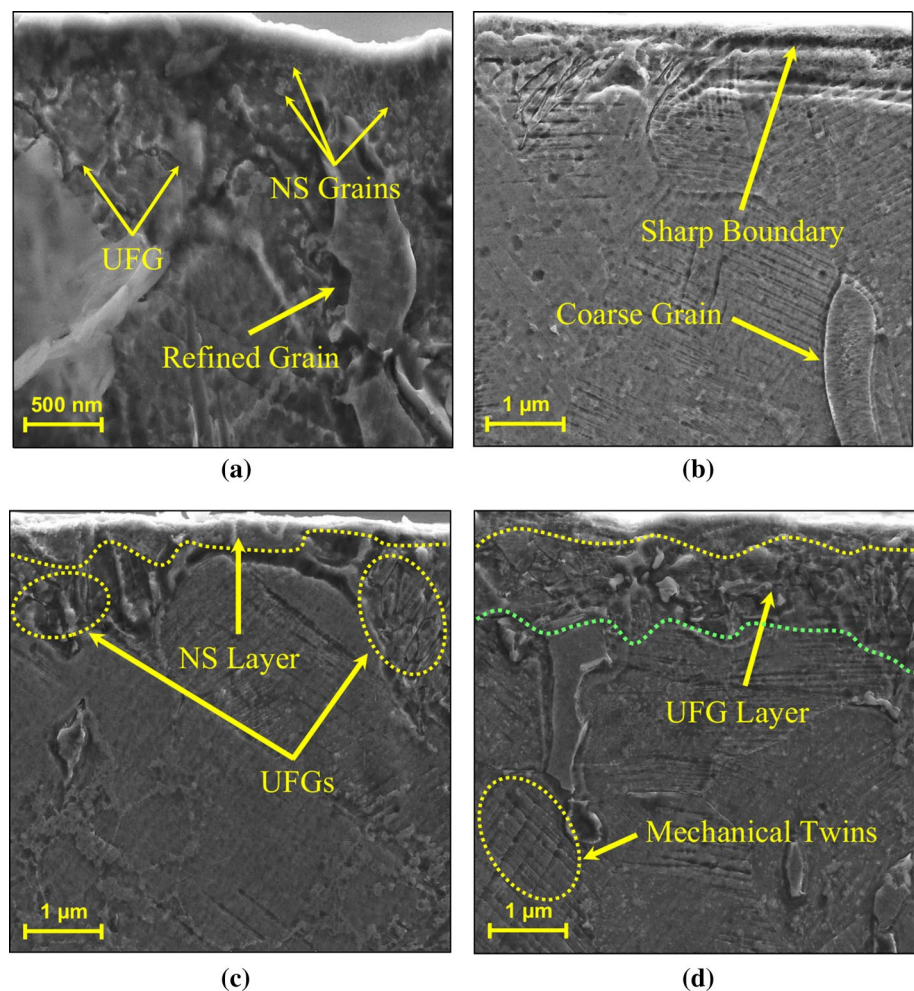


Table 5 FWHM and crystallite sizes of severely shot peened specimens with different intensities and same coverage of 1500%

| SSP treatment parameters | Peak | 2-Theta (°) | FWHM (°) | Crystallite size (nm) |
|--|---------|-------------|----------|-----------------------|
| Almen intensity: 12 A and coverage:1500% | (1 1 1) | 43.476 | 0.361 | 71.3 |
| Almen intensity: 15 A and coverage:1500% | (1 1 1) | 43.503 | 0.401 | 54.5 |
| Almen intensity: 18 A and coverage:1500% | (1 1 1) | 43.498 | 0.439 | 38.7 |
| Almen intensity: 21 A and coverage:1500% | (1 1 1) | 43.524 | 0.455 | 29.8 |
| Almen intensity: 24 A and coverage:1500% | (1 1 1) | 43.511 | 0.468 | 25.7 |
| Almen intensity: 27 A and coverage:1500% | (1 1 1) | 43.547 | 0.473 | 22.2 |

intensity of 21A and 500% coverage is shown in Appendix 2. The results of experimental measurements are presented in Fig. 9. It can be observed that both parameters of Almen intensity and surface coverage, directly related to one another, have a considerable influence on depth of the deformed layer (Fig. 9a, b). Surface roughness measurements (Fig. 9c) showed that by increasing surface coverage at a fixed intensity, roughness rises initially and then it is stabilized at the surface coverage of 200%–400%. However, it decreases at surface coverage of 1000%–1200%. Surface morphology of some shot peened specimens is illustrated in Appendix 3, confirming the roughness measurements. In the same coverage, intensity has a direct relation with roughness as well (as shown by FESEM observations in Fig. 6). Surface wettability of the shot peened steel 316L (Fig. 9d), as one of the main parameters of biocompatibility, decreased as the severity of SP process. Amount of the surface wettability can directly mediate the absorption of proteins to the implant surface and therefore, affect cell adhesion and its functions at the implant-tissue interface. Surface morphology and roughness and grain refinement are the main parameters that influence the surface contact area. In addition, surface energy and consequently enhancing the interaction of the substrate with the wetting medium have considerable effects [46]. The results indicated that the shot peened surface becomes more hydrophilic, with increased wettability observed, as its severity rises above the as-received material.

XRD stress measurements were employed to determine various distributions of residual stress in the treated specimens. For instance, in Fig. 6e, f, the residual stress distribution of shot peened specimens was compared under different Almen intensities of 12 and 21A by considering different values of coverage is presented. The as-received specimen (not shot peened) exerts approximately –25 MPa compressive residual stresses on the surface; however, more compressive residual stresses are induced in the surface layer with the application of SP treatments.

The magnitude of compressive residual stress (CRS) depends on the severity of SP process. In Fig. 6g, h, surface residual stress and maximum value of residual stress in depth are presented, respectively. It is evident that by increasing both Almen intensity and surface coverage, the

CRS value is enhanced. Nevertheless, as it can be clearly observed and as previously reported by Maleki et al. [26, 40, 42], Almen intensity has stronger effects than surface coverage on inducing residual stress.

5.2 RSM Results

The Almen intensity and surface coverage factors were determined by using ANOVA regression analysis. The effect and capability of the factors were evaluated for six responses (depth of deformed layer, surface ssmicrohardness, roughness, residual stress, and water contact angle). The factors and interactions were identified as “Almen intensity (A)”, “surface coverage (C)”, “Almen intensity*Almen intensity (A²)”, “surface coverage*surface coverage (C²)” and “Almen intensity*surface coverage (AC)”, respectively. The regression analysis was significant for all of the responses (Table 6). The P value extracted from the analysis points to the significance of the model under the value of 0.05. Otherwise, the factors and interactions should be defined as “insignificant” terms. The R-sq (%) of all responses exceeded 97%. Thus the model could be accepted as usable, and the outputs are predictable for the responses. The R-sq (adj) (%) and R-sq (pred) (%) pass 96% for all responses and demonstrates the significance of the model.

According to Table 6, surface coverage is the predominant factor in determining the deformed layer depth, as the P values of surface coverage prove its significance. Almen intensity by itself is an insignificant factor for the response. Figure 10a reveals the slope of the curves and distinguishes surface coverage as the principal factor. Surface microhardness is influenced positively by both factors due to its low P values. It is only the term “A²” which is insignificant for the model. Figure 10b shows that microhardness improves in a descending order through the severity of the factors individually. In other words, a harder layer could only be obtained with higher Almen intensities and at lower coverage values. The factors are significant except the term “AC” for surface roughness. However, the curves slope are nearly zero (horizontal) (Fig. 10c). Roughness remains largely stable, although coverage increases at a constant Almen intensity. The P value of surface coverage closer to

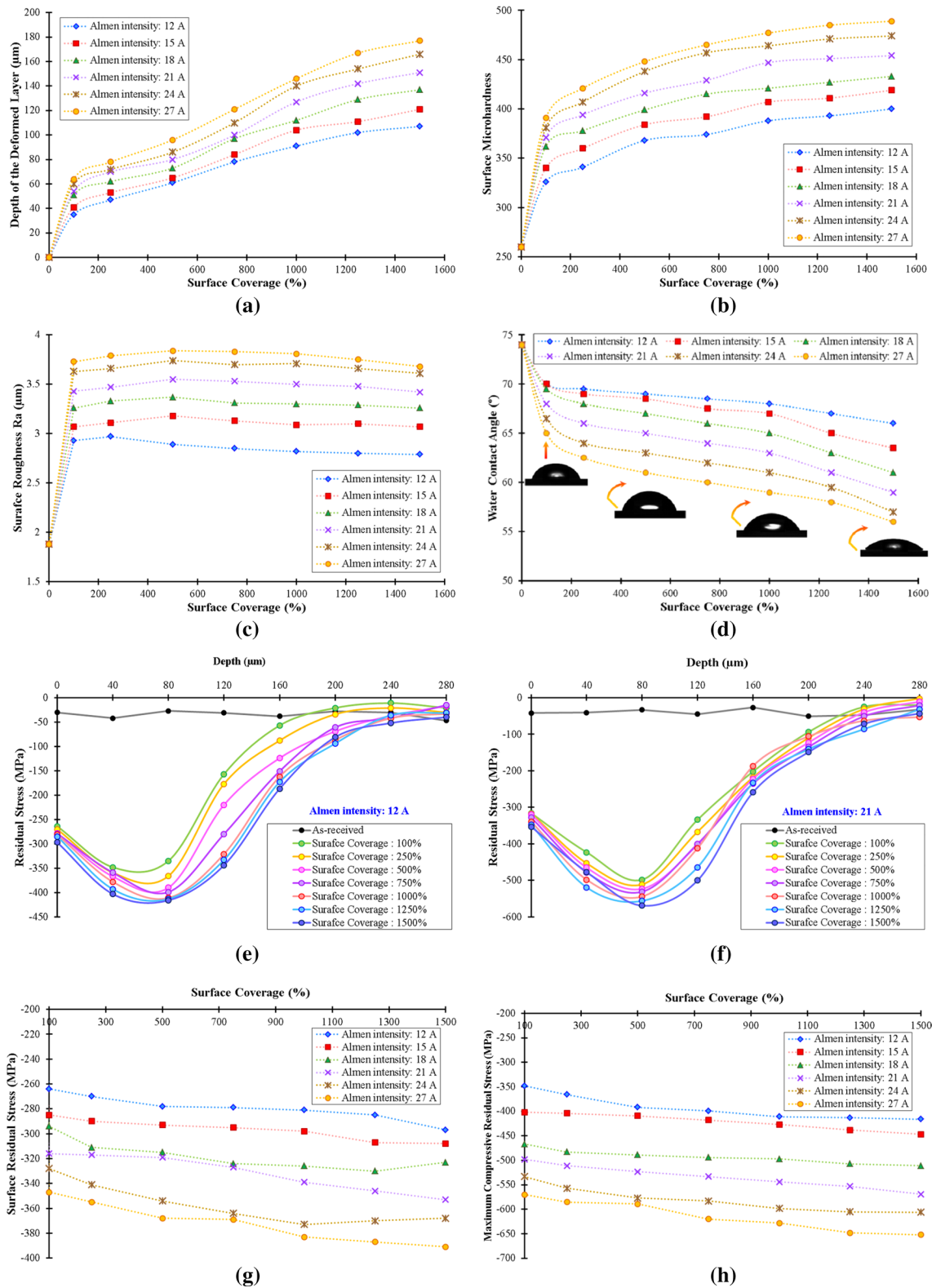


Fig. 9 Experimental measurements results for: **a** depth of deformed layer, **b** surface microhardness, **c** surface roughness, **d** surface wettability, **e** distribution of residual stress for shot peened specimens with intensity of 12 A and different coverages, **f** distribution of residual

stress for shot peened specimens with intensity of 21 A and different coverages, **g** surface residual stress, and **h** maximum value of residual stress

Table 6 Regression coefficients of the model for Almen intensity and surface coverage

| Inputs | P values for Outputs | | | | | |
|--|-------------------------|------------------------|-------------------|-------------------------|----------------------------------|---------------------|
| | Depth of deformed layer | Surface micro hardness | Surface roughness | Surface residual stress | Max. compressive residual stress | Water contact angle |
| Regression | 0.000 | 0.000 | 0.000 | 0.000 | 0.000 | 0.000 |
| Almen Intensity (0.001 mm A) | 0.013 | 0.000 | 0.000 | 0.002 | 0.000 | 0.533 |
| Surface Coverage (%) | 0.000 | 0.000 | 0.049 | 0.034 | 0.289 | 0.428 |
| Almen Intensity (0.001 mm A)* Almen Intensity (0.001 mm A) | 0.209 | 0.193 | 0.000 | 0.781 | 0.160 | 0.087 |
| Surface Coverage (%)*Surface Coverage (%) | 0.001 | 0.000 | 0.000 | 0.016 | 0.299 | 0.531 |
| Almen Intensity (0.001 mm A)* Surface Coverage (%) | 0.000 | 0.002 | 0.251 | 0.009 | 0.042 | 0.000 |
| Total | | | | | | |
| Model Summary | | | | | | |
| S value | 3.35067 | 4.55967 | 0.03545 | 4.77272 | 11.2249 | 0.6084 |
| R-sq (%) | 99.26 | 98.81 | 98.99 | 98.23 | 98.30 | 97.74 |

the critical boundary of significance expresses the behavior of the factor on roughness. The more effective parameter for residual stress exposure is Almen intensity (Fig. 10d). Surface coverage loses its effect substantially as a result of the exertion of maximum CRS (Fig. 10e). WCA regression analysis shows the only parameter that has a significant influence is the interaction of “AC”. Thus, Almen intensity and surface coverage have no remarkable effects individually. The increase of this interaction results in a lower impact than that obtained through WCA.

The RSM analysis was confirmed by six individual measurements (Table 7). The experiment and predicted results were compared and error percentage was evaluated. The predicted values were assessed for each response by regression equations (see Appendix 4). The arithmetic mean of errors was 2%. Error percentage was below 0.69% for surface microhardness individually and 1.34% for WCA. The confirmation tests provided by the model are consistent with different practical applications.

5.3 Taguchi Method Results

Taguchi sensitivity analysis was performed at every level of input parameters. The main effects of S/N ratios are plotted in Fig. 11. And the effect rate of each response in terms of various inputs is depicted in Fig. 12 (A and B symbols representing Almen intensity and surface coverage, respectively).

As shown in Fig. 12, Almen intensity is the more effective parameter for surface roughness, surface residual stress and maximum value of residual stress in depth. Conversely, the more effective parameter for depth of deformed layer is surface coverage. However, the effect of both input parameters is approximately equal for surface microhardness and wettability.

5.4 Optimization

In this study, Almen intensity and surface coverage were assessed as two inputs for the responses of deformed layer depth, surface microhardness, surface roughness, surface and maximum value of residual stress, and WCA alterations. The greater values of deformed layer, hardness and CRS afford a better SP process. On the contrary, the roughness values should be kept at their minimum intervals for dynamic applications. To this end, two different methods of RSM and TM were used to optimize SP parameters.

5.4.1 Optimization Through RSM

The optimization was carried out by Minitab Response Optimizer. The Almen intensity of 25.2183 (0.01 mm A) and surface coverage of 1500% were optimized with a composite desirability value of 0.7086 (Fig. 13). Given the optimized factors, maximum and surface CRSs were respectively optimized with -626.6756 and -379.5670 MPa, by overcoming the desirability value of 0.90. Surface hardness was optimized with 480.0854 HV, and depth of deformed layer reached 171.3848 μm .

5.4.2 Optimization Through TM

The optimization was undertaken by utilizing the results of Taguchi approach for 2 different cases. The purpose of the first case was to obtain optimal shot peening parameters and their corresponding output values by taking into account all the results of (R1-R6). But in the second case, which focused on the improvement of fatigue life, surface wettability was disqualified as an output. This is because each of the other outputs directly or indirectly affects fatigue life of

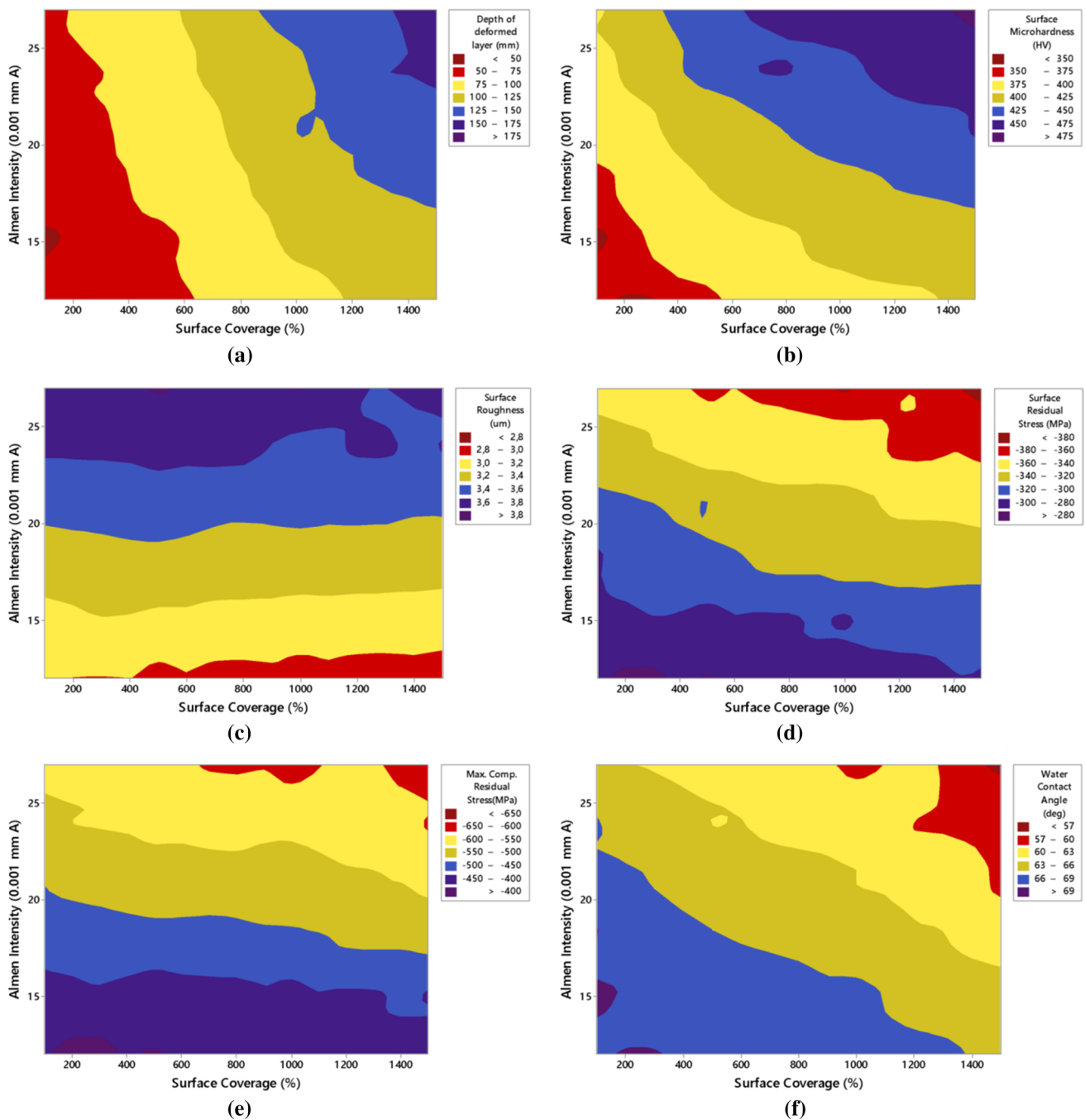


Fig. 10 The response surface 2D graphs of Almen intensity and surface coverage on the various responses: **a** depth of deformed layer, **b** surface microhardness, **c** surface roughness, **d** surface residual stress, **e** maximum compressive residual stress, and **f** water contact angle

components. The results of optimization analysis via Taguchi approach are reported in Table 8.

5.5 Fatigue Test Results

RSM determined that optimized Almen intensity is 25.2183A and the results of TM indicated that 26.12736A and 20.90548A are optimized values for two cases I and II,

respectively. The optimized value for surface coverage is 1500%, based on both methods. Therefore, three different treatments including 21-S1500, 24-S1500, and 27-S1500 were selected to investigate the effects of various surface treatments on the fatigue behavior of 316L stainless steel. The results of fatigue tests including S–N curves and fatigue limit of smooth and notched specimens are illustrated in Fig. 14.

Table 7 Confirmation of the tests and validity of the model

| Test no. | Inputs | | Outputs | | Confirmation Error (%) |
|--|------------------------------|----------------------|--------------|------------|------------------------|
| | Almen intensity (0.001 mm A) | Surface Coverage (%) | Experimental | Predicted | |
| Depth of deformed layer (mm) | | | | | |
| 1 | 12 | 100 | 35 | 36.7442 | 4.75 |
| 2 | 15 | 250 | 53 | 53.765 | 1.42 |
| 3 | 18 | 500 | 73 | 78.8834 | 7.46 |
| 4 | 21 | 750 | 100 | 105.2296 | 4.97 |
| 5 | 24 | 1000 | 140 | 132.8036 | 5.42 |
| 6 | 27 | 1250 | 167 | 161.6054 | 3.34 |
| Surface Microhardness (HV) | | | | | |
| 1 | 12 | 100 | 326 | 324.7994 | 0.37 |
| 2 | 15 | 250 | 360 | 357.52625 | 0.69 |
| 3 | 18 | 500 | 399 | 397.0272 | 0.49 |
| 4 | 21 | 750 | 429 | 431.62205 | 0.61 |
| 5 | 24 | 1000 | 464 | 461.3108 | 0.58 |
| 6 | 27 | 1250 | 485 | 486.09345 | 0.23 |
| Surface roughness Ra (μm) | | | | | |
| 1 | 12 | 100 | 2.93 | 2.857676 | 2.47 |
| 2 | 15 | 250 | 3.11 | 3.11915 | 0.29 |
| 3 | 18 | 500 | 3.37 | 3.377996 | 0.24 |
| 4 | 21 | 750 | 3.53 | 3.615314 | 2.42 |
| 5 | 24 | 1000 | 3.71 | 3.831104 | 3.26 |
| 6 | 27 | 1250 | 3.75 | 4.025366 | 7.34 |
| Surface Residual Stress (MPa) | | | | | |
| 1 | 12 | 100 | −264 | −265.0408 | 0.39 |
| 2 | 15 | 250 | −290 | −286.38625 | 1.25 |
| 3 | 18 | 500 | −315 | −311.2254 | 1.20 |
| 4 | 21 | 750 | −327 | −336.29185 | 2.84 |
| 5 | 24 | 1000 | −373 | −361.5856 | 3.06 |
| 6 | 27 | 1250 | −387 | −387.10665 | 0.03 |
| Max. Comp. Residual Stress (MPa) | | | | | |
| 1 | 12 | 100 | −348 | −365.5824 | 5.05 |
| 2 | 15 | 250 | −404 | −419.30625 | 3.79 |
| 3 | 18 | 500 | −489 | −476.4838 | 2.56 |
| 4 | 21 | 750 | −533 | −532.63345 | 0.07 |
| 5 | 24 | 1000 | −598 | −587.7552 | 1.71 |
| 6 | 27 | 1250 | −648 | −641.84905 | 0.95 |
| Water Contact Angle (deg) | | | | | |
| 1 | 12 | 100 | 70 | 70.94764 | 1.34 |
| 2 | 15 | 250 | 69 | 69.31975 | 0.46 |
| 3 | 18 | 500 | 67 | 66.95184 | 0.07 |
| 4 | 21 | 750 | 64 | 64.16531 | 0.26 |
| 5 | 24 | 1000 | 61 | 60.96016 | 0.07 |
| 6 | 27 | 1250 | 58 | 57.33639 | 1.16 |

Figure 14c presents a comparison of the fatigue limit of notched and un-notched specimens for all suggestions of optimized SP parameters based on RSM and TM. It should be noted that stress concentration coefficient is a key factor

which affects the notched fatigue results. This parameter is directly correlated with the reduction of cycles to failure, in comparison with smooth specimens. Similarly, if the same level of initial stress (associated with un-notched

Fig. 11 Effect of different input parameters on the **a** depth of deformed layer, **b** surface microhardness, **c** surface roughness, **d** surface residual stress, **e** maximum residual stress, and **f** surface wettability

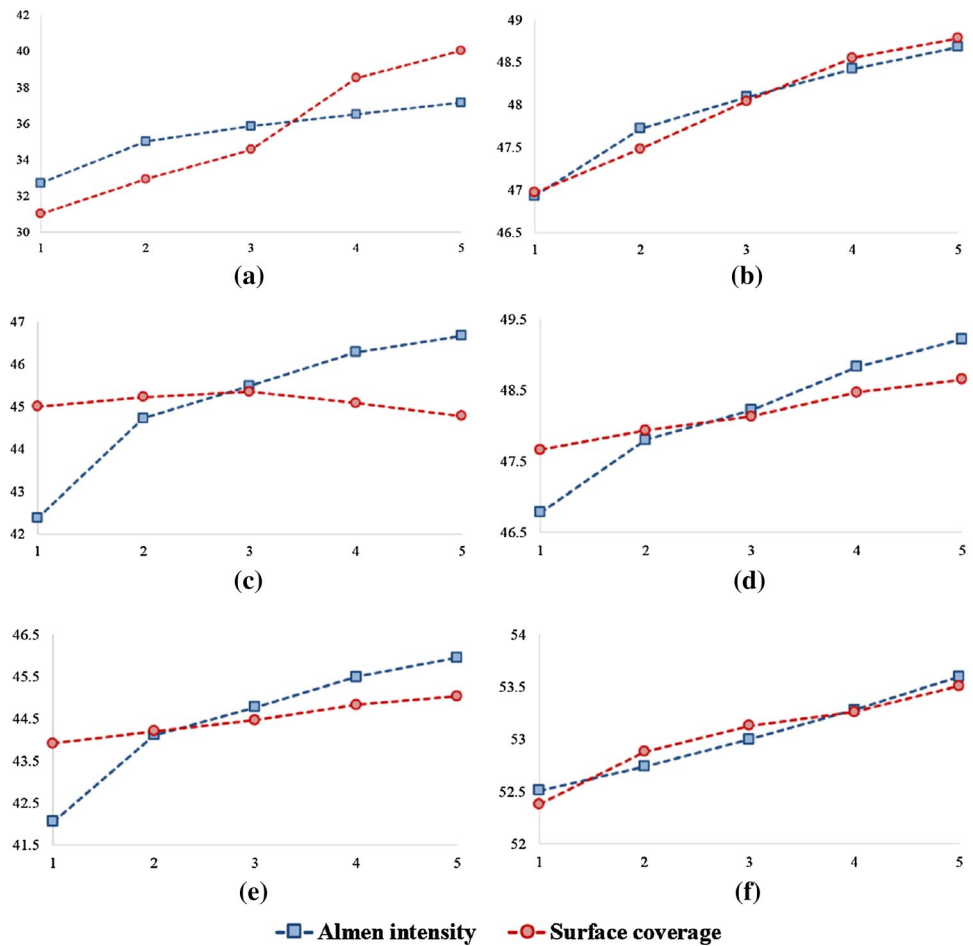
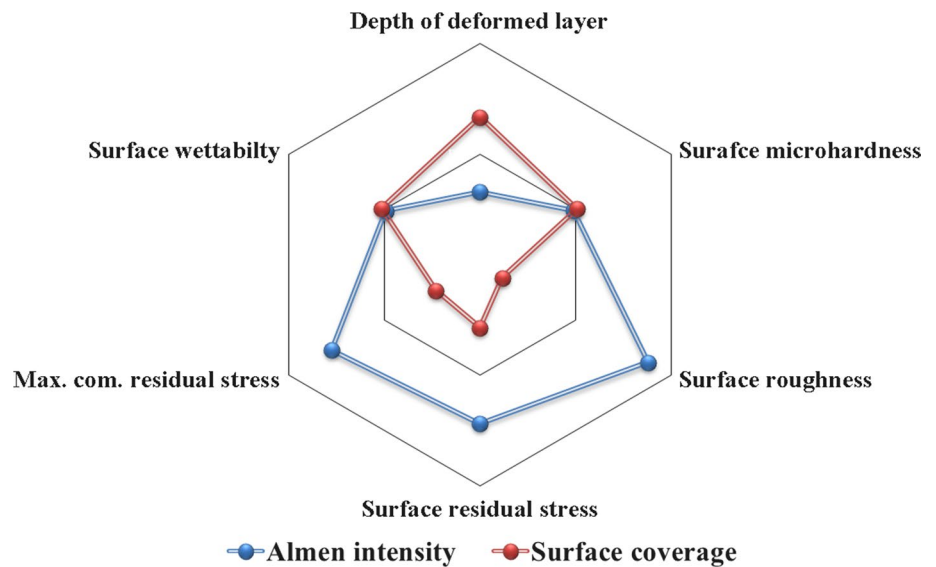


Fig. 12 Effect rate of each response in terms of different parameters of shot peening process using TM



samples) is used, the number of cycles to failure will be very low, even in the low-cycle region or where static failure occurs (one or more loading cycles). Hence, one of the common methods for comparing the fatigue limit of

these two samples (notched and un-notched) is to keep constant the number of cycles to failure and calculate the stress accordingly. In the present research, a large number

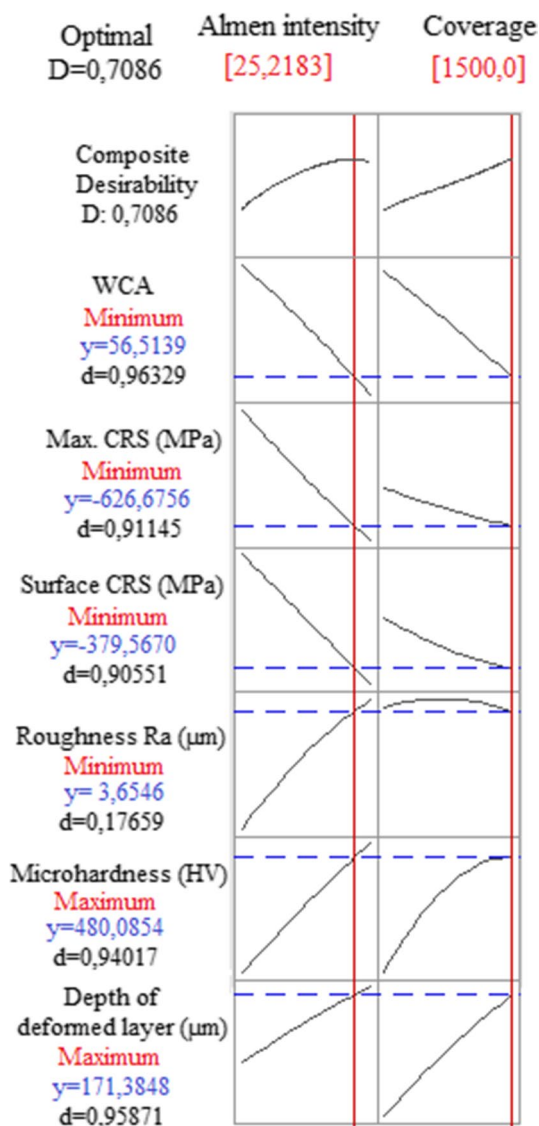


Fig. 13 The optimization of the model by RSM

of experiments were done to graphically compare the endurance fatigue limit of these two types of specimens.

As shown in Fig. 14 (S–N curves), the longest fatigue life is associated with severe shot peening treatment of 27-S1500, whose SP parameters were obtained via TM as the optimized values (for case I). Moreover, the fatigue limit of the 27-S1500 specimen is the highest in both modes of smooth and unnotched fatigue in comparison with other types of SP treatments. Table 9 summarizes the effects of different SP treatments on the fatigue strength of 316L stainless steel.

The results imply that SSP processes have been able to significantly improve fatigue strength, especially in the case of SSP: 27 A & 1500% treated specimens. Specially, 67.4208% and 81.25% enhancements were observed respectively for smooth and notched specimens. The data reported in Table 10 reveal that the influence of SP process on fatigue life improvement will rise by increasing the number of loading cycles. On the other hand, this treatment is more effective if lower stress amplitudes are applied. Moreover, fatigue strength improvement of notched specimens surpassed that smooth specimens in all cases examined. This finding shows that the effect of SP treatment in the crack growth stage is greater than that in the stage of crack germination. In other words, the consequence of this process on the crack growth rate is more significant than its effect on the overall life of the component (S–N).

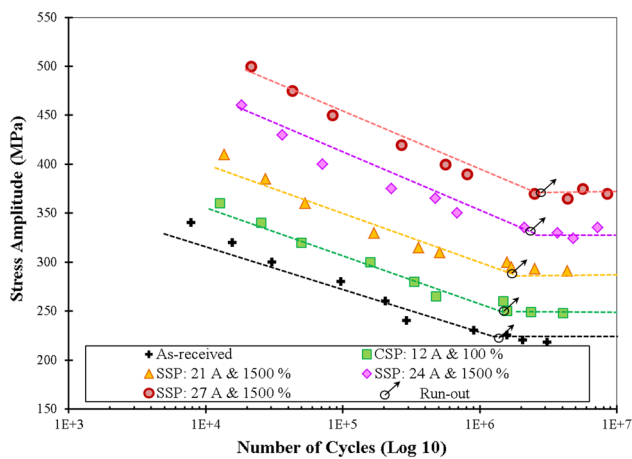
In addition, to have a better understanding about the mechanism of fatigue behavior of the treated specimens, the surface local fatigue of smooth specimens was calculated. This approach correlates the surface local fatigue strength to surface hardness and residual stress, which are generally determined for the surface-hardened material [78, 79]. The surface local fatigue strength is determined by utilizing the following relationship [80]:

$$X^* = \frac{1}{\sigma_{max}} \times \frac{d\sigma}{dx} \tag{13}$$

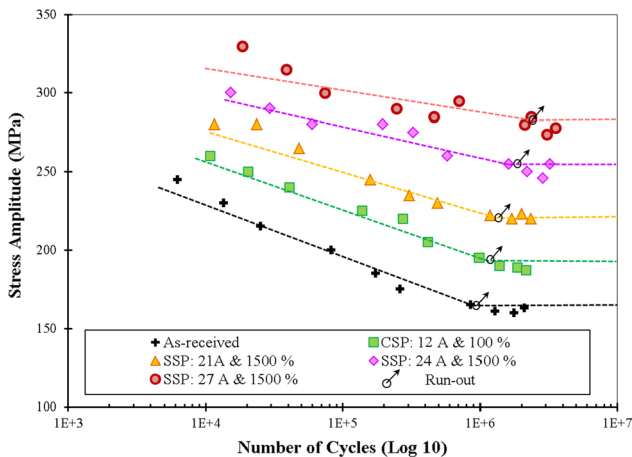
$$\sigma_{sw} = \sigma_{w0} \left(1 - \frac{\sigma_m + \sigma_{s,res}}{R_m} \right) \left(1 + \sqrt{\left(\frac{1600}{HV^2} \right) X^*} \right) \tag{14}$$

Table 8 Results of optimization analysis using TM

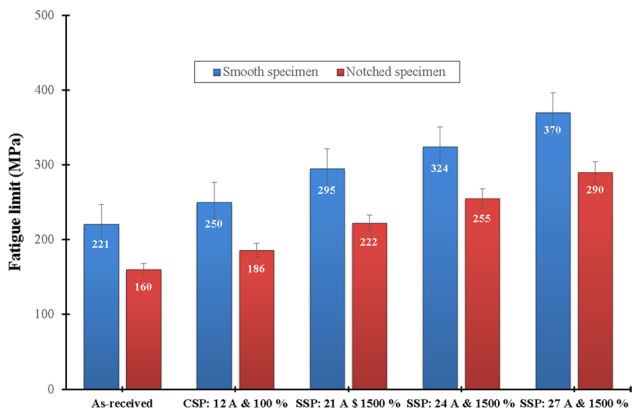
| Cases | | Unit | I | II |
|-------------------------------------|-------------------------|----------------|-----------|-----------|
| Optimized values (input parameters) | Almen intensity | A | 26.12736 | 20.90548 |
| | Surface coverage | % | 1500 | 1500 |
| Predicted values (output responses) | Depth of deformed layer | µm | 173.7591 | 160.5219 |
| | Surface microhardness | HV | 486.6986 | 467.3800 |
| | Surface roughness | µm | 3.6970 | 3.5510 |
| | Surface residual stress | MPa | -390.6198 | -365.4396 |
| | Maximum residual stress | MPa | -643.0487 | -603.357 |
| | Surface wettability | Degree (angle) | 55.9770 | - |



(a)



(b)



(c)

Fig. 14 Fatigue test results: **a** S–N curves for smooth specimens, **b** S–N curves for notched specimens, and **c** fatigue limit for both types of specimens

Table 9 Axial fatigue strength of 316L stainless steel considering the both smooth and notched specimens

| Fatigue specimen | Shot peening treatment | Fatigue limit improvement (%) |
|---------------------|------------------------|-------------------------------|
| Smooth (Un-Notched) | CSP: 12 A & 1500% | 13.12 |
| | SSP: 21 A & 1500% | 33.48 |
| | SSP: 24 A & 1500% | 46.60 |
| | SSP: 27 A & 1500% | 67.42 |
| Notched | CSP: 12 A & 1500% | 16.25 |
| | SSP: 21 A & 1500% | 38.75 |
| | SSP: 24 A & 1500% | 59.37 |
| | SSP: 27 A & 1500% | 81.25 |

where

$$R_m = 3.29 \times HV - 47, \text{ for } HV \leq 445 \quad (15a)$$

$$R_m = 4.02 \times HV - 374, \text{ for } HV > 445 \quad (15b)$$

$$\sigma_{w0} = 1.27 \times HV + 150, \text{ for } HV \leq 500 \quad (16)$$

$$\sigma_{w0} = 785, \text{ for } HV > 500 \quad (17)$$

where surface local fatigue (σ_{sw}), is considered to be a function of base fatigue limit (σ_{w0}), ultimate tensile strength (R_m), induced surface microhardness (H_V), surface residual stress ($\sigma_{s,res}$), mean applied stress (σ_m), as well as applied relative stress gradient (X^*). It was obtained about 787 MPa for the conventional SP process. The relative values of surface local fatigue of smooth specimens are depicted in Fig. 15. It can be observed that besides the results of the experiments, theoretically by increasing the severity of SP process, heightens the required stress for crack initiation.

6 Summary and Conclusion

In the present research, a comprehensive study was undertaken on the shot peening of steel AISI 316 L biomaterial. A total of 42 different SP treatments with varying Almen intensities of 12–27 A and various coverage degrees of 100–1500% (from conventional to severe) were applied to experimentally investigate the mechanical properties of 316L biomaterial. The experimental results revealed that increasing SP severity, is followed by a rise in the depth of plastically deformed layer, surface microhardness, surface residual stress and maximum compressive residual stress, but a considerable drop in the water contact angle. Moreover, the rise of SP severity causes surface roughness increase initially, yet a further SP severity stabilizes surface

Table 10 Details of the obtained results of sensitivity analysis and optimization via different approaches of RSM and TM

| Utilized approach | Considered output | Sensitivity analysis (%) | | Optimization | |
|-------------------|-------------------------|--------------------------|------------------|-----------------------------|----------------------|
| | | Almen intensity | Surface coverage | Almen intensity (0.01 mm A) | Surface coverage (%) |
| RSM | Depth of deformed layer | – | – | 25.2183 | 1500 |
| | Surface microhardness | – | – | | |
| | Surface roughness | – | – | | |
| | Surface residual stress | – | – | | |
| | Maximum CRS | – | – | | |
| | Surface wettability | – | – | | |
| TM | Depth of deformed layer | 33 | 67 | Case I | 26.12736 1500 |
| | Surface microhardness | 49 | 51 | | |
| | Surface roughness | 88 | 12 | | |
| | Surface residual stress | 72 | 28 | Case II | 20.90548 1500 |
| | Maximum CRS | 77 | 23 | | |
| | Surface wettability | 49 | 51 | | |

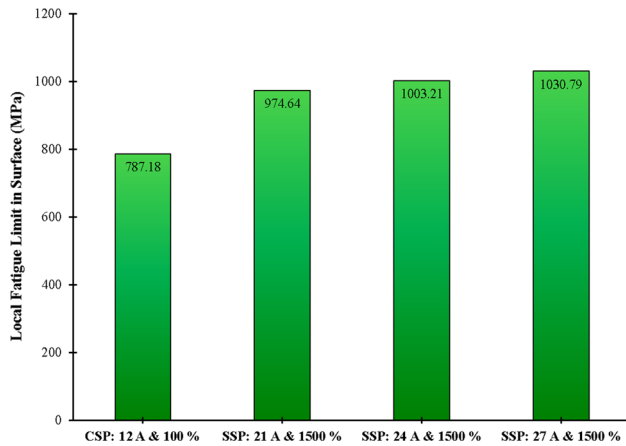


Fig. 15 Surface local fatigue of smooth specimens

roughness. Eventually, in the third step, surface roughness falls as a result of SP severity.

Two different methods of response surface morphology, and Taguchi method were utilized for parametric analysis and optimization which were conducted based on the experimental results. The results of the three approaches are largely in line have very good agreement with experimental results. Parametric analysis demonstrated that heightening Almen intensity and surface coverage plays a considerable role in the increase of the depth of plastically deformed layer, surface hardening and rising of induced compressive residual stress. Parametric analysis of surface roughness showed that intensity of peening has a greater effect than surface coverage; also, it can be seen that increasing surface coverage leads to a

reduction in roughness. On the other hand, by enhancing the inputs, surface wettability decreases and becomes more hydrophilic.

Moreover, sensitivity analysis determined the effective parameters and the SP process was optimized according to the experiments. Table 10 summarizes the related results; TM was used for sensitivity analysis to achieve the relative importance of the each input parameters.

Finally, after optimization and determination of the optimal values of Almen intensity and coverage through two approaches of RSM and TM, different smooth and notched fatigue specimens were prepared with desirable conditions to investigate the fatigue behavior via axial fatigue tests. The results illustrated that the SSP processes improve fatigue strength significantly. This was particularly the case for SSP: 27A & 1500% treated specimens, which revealed enhancements of 67.4208% and 81.25% for smooth and notched specimens, respectively.

It can be concluded that if alternative approaches such as RSM and TM are adjusted carefully, it is possible to achieve results that approximate experimental observations. Hence, these approaches can be employed as powerful tools for modelling, analyzing and optimizing widely used processes such as SP.

Appendixes

Appendix 1

See Fig. 16.

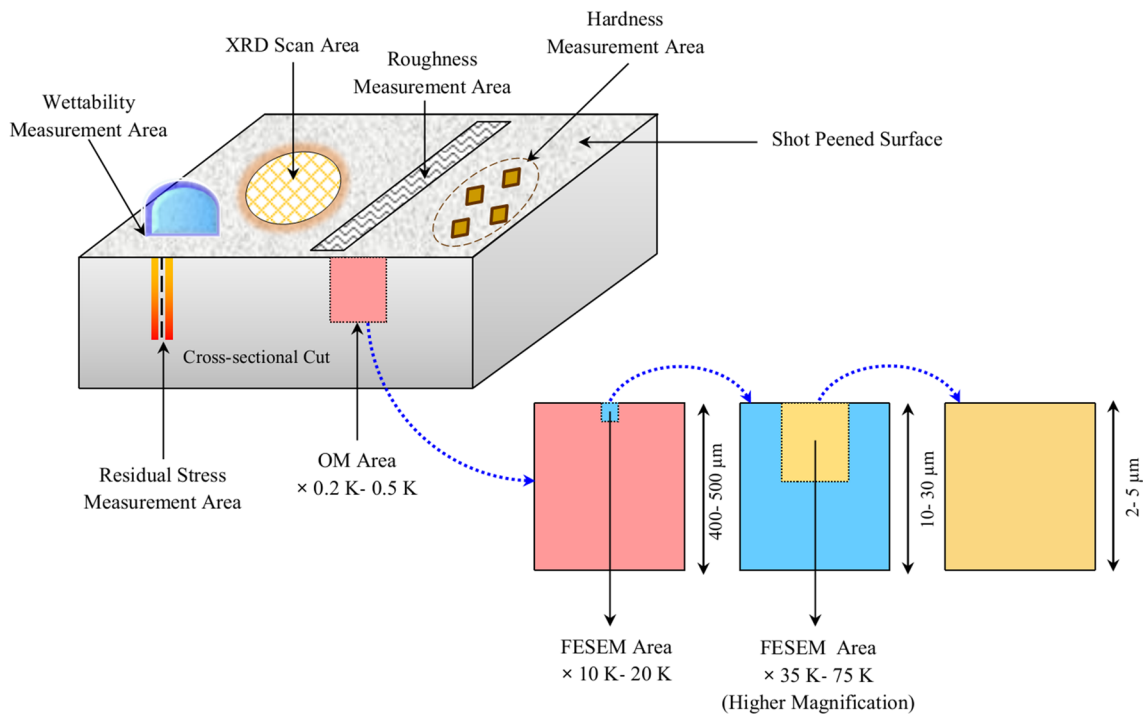


Fig. 16 Scanning area of the different applied experiments

Appendix 2

See Fig. 17.

Appendix 3

See Fig. 18.

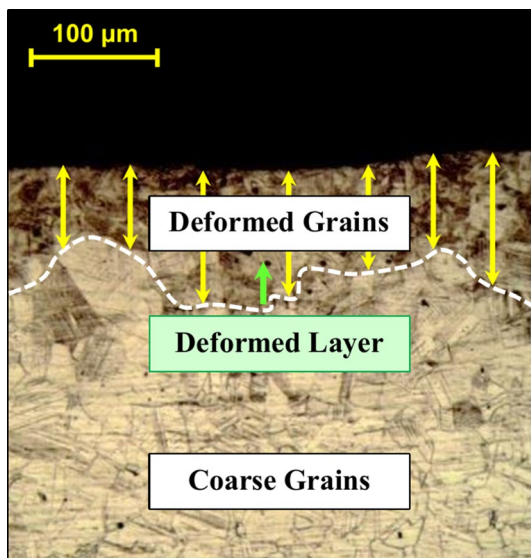


Fig. 17 Measurement of the depth of the deformed layer in the shot peened specimen with intensity of 21 A and 500% coverage

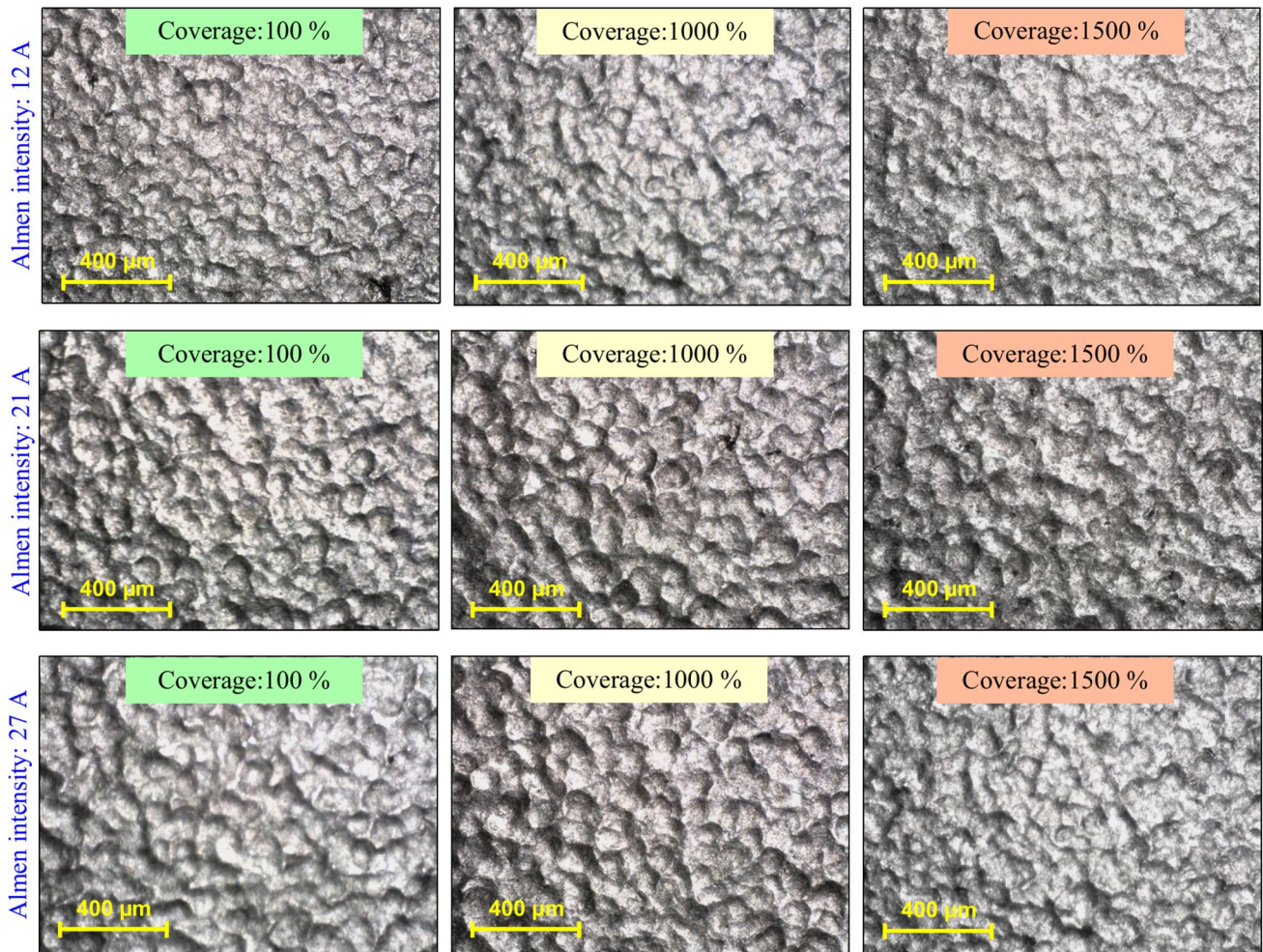


Fig. 18 Surface morphology of shot peened specimens with intensities of 12, 21 and 27 A with different coverage of 100, 1000 and 1500%

Appendix 4

Regression Equations for RSM

Depth of deformed layer (mm) = $1.9 + 2.72 \text{ Almen Intensity (0.001 mm A)} + 0.04431 \text{ Surface Coverage (\%)} - 0.0324 \text{ Almen Intensity (0.001 mm A)} * \text{Almen Intensity (0.001 mm A)} - 0.000011 \text{ Surface Coverage (\%)} * \text{Surface Coverage (\%)} + 0.002124 \text{ Almen Intensity (0.001 mm A)} * \text{Surface Coverage (\%)}$.

Surface Microhardness (HV) = $240.5 + 6.67 \text{ Almen Intensity (0.001 mm A)} + 0.10807 \text{ Surface Coverage (\%)} - 0.0457 \text{ Almen Intensity (0.001 mm A)} * \text{Almen Intensity (0.001 mm A)} - 0.000046 \text{ Surface Coverage (\%)} * \text{Surface Coverage (\%)} + 0.001111 \text{ Almen Intensity (0.001 mm A)} * \text{Surface Coverage (\%)}$.

Surface Roughness (μm) = $1.655 + 0.1160 \text{ Almen Intensity (0.001 mm A)} + 0.000153 \text{ Surface Coverage (\%)} - 0.001446 \text{ Almen Intensity (0.001 mm A)} * \text{Almen Intensity (0.001 mm A)}$

$- 0.000000 \text{ Surface Coverage (\%)} * \text{Surface Coverage (\%)} + 0.000003 \text{ Almen Intensity (0.001 mm A)} * \text{Surface Coverage (\%)}$.

Surface Residual Stress (MPa) = $-199.0 - 5.11 \text{ Almen Intensity (0.001 mm A)} - 0.0224 \text{ Surface Coverage (\%)} - 0.0101 \text{ Almen Intensity (0.001 mm A)} * \text{Almen Intensity (0.001 mm A)} + 0.000011 \text{ Surface Coverage (\%)} * \text{Surface Coverage (\%)} - 0.000947 \text{ Almen Intensity (0.001 mm A)} * \text{Surface Coverage (\%)}$.

Max. Comp. Residual Stress (MPa) = $-154.6 - 18.67 \text{ Almen Intensity (0.001 mm A)} - 0.0256 \text{ Surface Coverage (\%)} + 0.1218 \text{ Almen Intensity (0.001 mm A)} * \text{Almen Intensity (0.001 mm A)} + 0.000011 \text{ Surface Coverage (\%)} * \text{Surface Coverage (\%)} - 0.001693 \text{ Almen Intensity (0.001 mm A)} * \text{Surface Coverage (\%)}$.

Water Contact Angle (deg.) = $73.85 - 0.118 \text{ Almen Intensity (0.001 mm A)} - 0.00103 \text{ Surface Coverage (\%)} - 0.00809 \text{ Almen Intensity (0.001 mm A)} * \text{Almen Intensity (0.001 mm A)}$

Intensity (0.001 mm A) – 0.000000 Surface Coverage (%) *Surface Coverage (%) – 0.000182 Almen Intensity (0.001 mm A) *Surface Coverage (%).

Funding Open access funding provided by Politecnico di Milano within the CRUI-CARE Agreement.

Declarations

Conflict of interest The authors declare that they have no conflict of interest.

Open Access This article is licensed under a Creative Commons Attribution 4.0 International License, which permits use, sharing, adaptation, distribution and reproduction in any medium or format, as long as you give appropriate credit to the original author(s) and the source, provide a link to the Creative Commons licence, and indicate if changes were made. The images or other third party material in this article are included in the article's Creative Commons licence, unless indicated otherwise in a credit line to the material. If material is not included in the article's Creative Commons licence and your intended use is not permitted by statutory regulation or exceeds the permitted use, you will need to obtain permission directly from the copyright holder. To view a copy of this licence, visit <http://creativecommons.org/licenses/by/4.0/>.

References

1. A.L. Garcia-Garcia, M. Alvarez-Vera, L.A. Montoya-Santianes, I. Dominguez-Lopez, J.L. Montes-Seguedo, J.C. Sosa-Savedra, J.D.O. Barceinas-Sanchez, *J. Mech. Behav. Biomed.* **82**, 248 (2018)
2. F. Hosseinzadeh, S. Hossain, C.E. Truman, D.J. Smith, *Exp. Mech.* **54**, 1151 (2014)
3. L. Gil, S. Brühl, L. Jiménez, O. Leon, R. Guevara, M.H. Staia, *Surf. Coat. Tech.* **201**, 4424 (2006)
4. J.V. Stolen, L. Labey, R.V. Audekercke, G.V. der Perre, *Biomaterials* **19**, 1455 (1998)
5. Z. Sun, X. Tan, S.B. Tor, W.Y. Yeong, *Mater. Design* **104**, 197 (2016)
6. J. Suryawanshi, K.G. Prashanth, U. Ramamurty, *Mater. Sci. Eng. A* **696**, 113 (2017)
7. T. Kurzynowski, K. Gruber, W. Stopyra, B. Kuźnicka, E. Chlebus, *Mater. Sci. Eng. A* **718**, 64 (2018)
8. E. Maleki, N. Maleki, A. Fattahi, O. Unal, M. Guagliano, S. Bagherifard, *Surf. Coat. Tech.* **405**, 126729 (2021)
9. K. Benarji, Y. Ravi Kumar, A.N. Jinoop, C.P. Paul, K.S. Bindra, *Met. Mater. Int.* **27**, 488 (2021)
10. M. Mamivand, Y. Yang, J. Busby, D. Morgan, *Acta Mater.* **130**, 94 (2017)
11. K. Saeidi, X. Gao, Y. Zhong, Z.J. Shen, *Mater. Sci. Eng. A* **625**, 221 (2015)
12. N.P. Lavery, J. Cherry, S. Mehmood, H. Davies, B. Girling, E. Sackett, S.G.R. Brown, J. Sienz, *Mater. Sci. Eng. A* **693**, 186 (2017)
13. R.D. Monteiro, J. van de Wetering, B. Krawczyk, D.L. Engelberg, *Met. Mater. Int.* **26**, 630 (2020)
14. A. Röttger, K. Geenen, M. Windmann, F. Binner, W. Theisen, *Mater. Sci. Eng. A* **678**, 365 (2016)
15. H.D. Carlton, A. Haboub, G.F. Gallegos, D.Y. Parkinson, A.A. MacDowell, *Mater. Sci. Eng. A* **651**, 406 (2016)
16. I. Tolosa, F. Garciandía, F. Zubiri, F. Zapirain, A. Esnaola, *Int. J. Adv. Manuf. Tech.* **51**, 639 (2010)
17. B.H. Sencer, S.A. Maloy, G.T. Gray, *Acta Mater.* **53**, 3293 (2005)
18. E. Maleki, O. Unal, K.R. Kashyzadeh, *Mater. Charact.* **157**, 109877 (2019)
19. H. Gleiter, *Acta Mater.* **48**, 1 (2000)
20. M.A. Meyers, A. Mishra, D.J. Benson, *Prog. Mater. Sci.* **51**, 427 (2006)
21. Y. Efe, I. Karademir, F. Husem, E. Maleki, R. Karimbaev, A. Amanov, O. Unal, *Appl. Surf. Sci.* **528**, 146922 (2020)
22. E. Maleki, O. Unal, K.R. Kashyzadeh, *Met. Mater. Int.* **25**, 1436 (2019)
23. O. Unal, E. Maleki, *Measurement* **125**, 133 (2018)
24. E. Maleki, O. Unal, A. Amanov, *Surf. Interfaces* **13**, 233 (2018)
25. E. Maleki, O. Unal, Optimization of shot peening effective parameters on surface hardness improvement. *Met. Mater. Int.* (2020). <https://doi.org/10.1007/s12540-020-00758-x>
26. E. Maleki, O. Unal, K.R. Kashyzadeh, *Surf. Coat. Tech.* **344**, 62 (2018)
27. B. Sagbas, *Met. Mater. Int.* **26**, 143 (2020)
28. E. Maleki, S. Bagherifard, M. Bandini, M. Guagliano, *Addit. Manuf.* **37**, 101619 (2021)
29. E. Maleki, O. Unal, Fatigue limit prediction and analysis of nano-structured AISI 304 steel by severe shot peening via ANN. *Eng. Comput.* (2020). <https://doi.org/10.1007/s00366-020-00964-6>
30. E. Maleki, O. Unal, *Met. Mater. Int.* **27**, 262 (2021)
31. O. Unal, E. Maleki, R. Varol, *Vacuum* **150**, 69 (2018)
32. Y. Wang, H. Yang, C. Zhan, F. Yu, *Met. Mater. Int.* **21**, 260 (2015)
33. A. Amanov, R. Karimbaev, E. Maleki, O. Unal, Y.-S. Pyun, T. Amanov, *Surf. Coat. Tech.* **358**, 695 (2019)
34. N.R. Tao, Z.B. Wang, W.P. Tong, M.L. Sui, J. Lu, K. Lu, *Acta Mater.* **50**, 4603 (2002)
35. K. Lu, J. Lu, *Mater. Sci. Eng. A* **375-377**, 38 (2004)
36. E. Maleki, G.H. Farrahi, K.R. Kashyzadeh, O. Unal, M. Guagliano, S. Bagherifard, *Met. Mater. Int.* **27**, 2575 (2021)
37. O. Unal, A. Cahit Karaoglanli, R. Varol, A. Kobayashi, *Vacuum* **110**, 202 (2014)
38. S.M. Hassani-Gangaraj, K.S. Choa, H.J.L. Voigt, M. Guagliano, C.A. Schuh, *Acta Mater.* **97**, 105 (2015)
39. Q. Zhou, R. Wang, Z. Zheng, Y. Gao, *Appl. Surf. Sci.* **462**, 804 (2018)
40. E. Maleki, O. Unal, *Surf. Interfaces* **11**, 82 (2018)
41. E. Maleki, G.H. Farrahi, *Int. J. Eng. Trans. B: Appl.* **31**, 382 (2018)
42. E. Maleki, O. Unal, K.R. Kashyzadeh, *Int. J. Fatigue* **116**, 48 (2018)
43. S. Bagherifard, D.J. Hickey, S. Fintová, F. Pastorek, I. Fernandez-Pariente, M. Bandini, T.J. Webster, M. Guagliano, *Acta Biomater.* **66**, 93 (2018)
44. A. Al-Janabi, M.R. Malayeri, O.O. Badran, *Int. J. Therm. Sci.* **111**, 379 (2017)
45. S. Bagherifard, S. Slawik, I. Fernández-Pariente, C. Pauly, F. Mücklich, M. Guagliano, *Mater. Design* **102**, 68 (2016)
46. S. Bagherifard, D.J. Hicke, A.C. de Luca, V.N. Malheiro, A.E. Markaki, M. Guagliano, T.J. Webster, *Biomaterials* **73**, 185 (2015)
47. J.-S. Li, W.-D. Gao, Y. Cao, Z.O.W. Huang, B. Gao, Q.Z. Mao, Y.S. Li, *Adv. Eng. Mater.* **20**, 1800402 (2018)
48. ASTM E8-04, Standard Test Methods for Tension Testing of Metallic Materials (ASTM International, West Conshohocken, 2004)

49. ASTM E466-15, Standard Practice for Conducting Force Controlled Constant Amplitude Axial Fatigue Tests of Metallic Materials (ASTM International, West Conshohocken, 2015)
50. SAE J443_198401, Procedures for Using Standard Shot Peening Almen test strip (SAE International, Warrendale, 1984)
51. C. Suryanarayana, M.G. Norton, *X-Ray Diffraction a Practical Approach* (Plenum Press, New York, 1998)
52. ISO 4278, Geometrical Product Specifications (GPS) – Surface Texture: Profile Method-Terms, Definitions and Surface Texture Parameters (International Organization for Standardization, Geneva, 1997)
53. K.R. Kashyzadeh, E. Maleki, J. Fail. Anal. Prev. **17**, 1276 (2017)
54. U. Karr, R. Schuller, M. Fitzka, B. Schönbauer, D. Tran, B. Penning, H. Mayer, J. Mater. Sci. **52**, 5954 (2017)
55. E. Maleki, O. Unal, M. Guagliano, S. Bagherifard, Mater. Sci. Eng.: A. **810**, 141029 (2021)
56. JSME S002, Standard Method of Statistical Fatigue Testing (The Japan Society of Mechanical Engineers, Tokyo, 1981)
57. A.R. Hamad, J.H. Abboud, F.M. Shuaeib, K.Y. Benyounis, Adv. Eng. Softw. **41**, 674 (2010)
58. İ Asiltürk, S. Neşeli, Measurement **45**, 785 (2012)
59. V. Vembu, G. Ganesan, Def. Technol. **11**, 390 (2015)
60. O. Unal, Surf. Coat. Tech. **305**, 99 (2016)
61. Y.-S. Nam, Y.-I. Jeong, B.-C. Shin, J.-H. Byun, Mater. Design **83**, 566 (2015)
62. Y.Q. Sun, J.Z. Zhou, Y.B. Chen, S. Huang, Appl. Mech. Mater. **10–12**, 692 (2008)
63. A. Pathak, K. Munjadas, IOSR J. Mech. Civ. Eng. **14**, 60 (2017)
64. K. Thirumavalavan, L. Karunamoorthy, K.A. Padmanabhan, Int. J. Eng. Technol. **6**, 1026 (2014)
65. H. Jamaluddin, J.A. Ghani, B. Md Deros, M.N. Ab Rahman, R. Ramli, J. Mech. Eng. Sci. **10**, 2200 (2016)
66. L. Singh, R.A. Khan, M.L. Aggarwal, J. Mech. Sci. Technol. **26**, 1731 (2012)
67. P.M. George, N. Pillai, N. Shah, J. Mater. Process. Tech. **153–154**, 925 (2004)
68. S. Elyaskhani, M.A. Moyeed, M.S. Seddiqui, G.M. SayeedAhmed, M.M.A. Baig, Mater. Today **2**, 3363 (2015)
69. K. Li, S. Yan, Y. Zhong, W. Pan, G. Zhao, Simul. Model. Pract. Th. **91**, 69 (2019)
70. A. Qasim, S. Nisar, A. Shah, M.S. Khalid, M.A. Sheikh, Simul. Model. Pract. Th. **59**, 36 (2015)
71. G.M. Lule Senoz, T.A. Yilmaz, Met. Mater. Int. **27**, 436 (2021)
72. T. Thankachan, K. Soorya Prakash, V. Kavimani, S.R. Silambarasan, Met. Mater. Int. **27**, 220 (2021)
73. A. Chamanfar, H. Monajati, A. Rosenbaum, M. Jahazi, A. Bonakdar, E. Morin, Mater. Charact. **132**, 53 (2017)
74. A. Zammit, S. Abela, L. Wagner, M. Mhaede, R. Wan, M. Grech, Surf. Coat. Tech. **308**, 213 (2016)
75. H. Saitoh, T. Ochi, M. Kubota, in *Proceedings of the 10th International Conference on Shot Peening*, Japan, 15–18 September 2008, pp. 488–493
76. K.A. Soady, B.G. Mellor, G.D. West, G. Harrison, A. Morris, P.A.S. Reed, Int. J. Fatigue **54**, 106 (2013)
77. E. Maleki, O. Unal, M. Guagliano, S. Bagherifard, Analysing the fatigue behaviour and residual stress relaxation of gradient nanostructured 316L steel subjected to the shot peening via deep learning approach. Met. Mater. Int. (2021). <https://doi.org/10.1007/s12540-021-00995-8>
78. P. De La Cruz, M. Oden, T. Ericsson, Int. J. Fatigue **20**, 389 (1998)
79. S. Kikuchi, Y. Nakahara, J. Komotori, Int. J. Fatigue **32**, 403 (2010)
80. E. Maleki, O. Unal, K.R. Kashyzadeh, S. Bagherifard, M. Guagliano, Appl. Surf. Sci. Adv. **4**, 100071 (2021)

Publisher's Note Springer Nature remains neutral with regard to jurisdictional claims in published maps and institutional affiliations.